CFD MODELLING OF DRILL CUTTINGS TRANSPORT EFFICIENCY IN ANNULAR BENDS: EFFECT OF HOLE ECCENTRICITY AND ROTATION.

M. Nur Alam Zico

MASTER OF ENGINEERING IN PETROLEUM ENGINEERING

DEPARTMENT OF PETROLEUM AND MINERAL RESOURCES ENGINEERING
BANGLADESH UNIVERSITY OF ENGINEERING AND TECHNOLOGY
DHAKA-1000, BANGLADESH

October 2021

CFD MODELLING OF DRILL CUTTINGS TRANSPORT EFFICIENCY IN ANNULAR BENDS: EFFECT OF HOLE ECCENTRICITY AND ROTATION.

A Project

By

M. Nur Alam Zico

Roll NO: 1015132002

Submitted to the

Department of Petroleum and Mineral Resources Engineering

In partial fulfilment of requirements for the degree of

MASTER OF ENGINEERING IN PETROLEUM ENGINEERING

DEPARTMENT OF PETROLEUM AND MINERAL RESOURCES ENGINEERING
BANGLADESH UNIVERSITY OF ENGINEERING AND TECHNOLOGY
DHAKA-1000, BANGLADESH

October 2021

RECOMEDATION OF THE BOARD OF EXAMINERS

The project entitled as **"CFD Modelling Of Drill Cuttings Transport Efficiency In Annular Bends: Effect Of Hole Eccentricity And Rotation"** submitted by M. Nur Alam Zico, Roll No: 1015132002, Session: October 2015, has been accepted as satisfactory in partial fulfillment of the requirements for the degree of **Master of Engineering In Petroleum Engineering**.

Chairman (Supervisor): _____

Hazzaz Bin Yousuf
Assistant Professor,
Department of Petroleum and Mineral Resources Engineering,
Bangladesh University of Engineering and Technology,
Dhaka.

Member : _____

Dr. Mohammed Mahbubur Rahman
Professor and Head,
Department of Petroleum and Mineral Resources Engineering,
Bangladesh University of Engineering and Technology,
Dhaka.

Member : _____

Dr. Mohammad Tamim
Professor,
Department of Petroleum and Mineral Resources Engineering,
Bangladesh University of Engineering and Technology,
Dhaka.

Date: October 30, 2021

DECLARATION

It is hereby declared that this project or any part of it has not been submitted to elsewhere for the award of any other degree.

M. Nur Alam Zico

ABSTRACT

Increasing the cuttings transport performance in deviated wells is difficult due to the rolling transport and cuttings settling on the low side of the annulus. Insufficient cuttings transport may lead to some crucial problems such as pipe sticking, increasing in torque and drag, material damage and bed cementing quality. Increasing flow rates and improving mud properties may not be applicable for a proper hole cleaning because of the hydraulic and mechanical limitations. In such cases, additional pressure may be generated, and this causes formation fractures and drilling fluid losses. Under these circumstances, the other major contribution to cuttings transport is provided by drill-pipe rotation for different eccentricity. This project describes the relation between hole eccentricity and rotation during cuttings transport through annular bends.

The present study focused on the development of a computational fluid dynamics model to predict these parameters conveniently and accurately. Two phases—liquid (water) and cuttings (sulfur solid)—were considered. The simulations were conducted using the workbench platform of ANSYS Fluent 2021 R1. The Eulerian model of multiphase flow and the Reynolds stress model of turbulence closure available in Fluent were used for the present study. The average velocities and volumetric concentrations of involved phases were specified as the inlet boundary conditions. The stationary surfaces of the flow channels were hydrodynamically considered as either smooth or rough walls, and the outlets were regarded as being open to the atmosphere. The simulation results of pressure loss showed a good agreement with the predictions of well-established correlations.

From the simulated results, this project concludes that drill cuttings transport efficiency depends on hole eccentricity and drill pipe rotation of the models where pressure and VOF of cuttings are maximum with minimum pressure drop. For eccentricity 0.4 with 200 rpm simulation shows maximum pressure at outlet with maximum cuttings VOF and also shows minimum pressure drop than other models at outlet.

ACKNOWLEDGMENTS

This work has been carried out as our Project of Master of Engineering In Petroleum Engineering in Bangladesh University of Engineering and Technology (BUET). Our intense gratefulness goes to almighty Allah for His divine blessings over us.

We would like to sincerely thank our supervisor Assistant Professor Hazzaz Bin Yousuf who guided us to find a subject for the thesis and gave us a perfect description of the subject, which was a great help later finding our way to do our thesis. Again, thanks to Shahriar Mahmud, Assistant Professor, Department of Petroleum and Mineral Resource Engineering, BUET and Sheikh Zahidul Islam, Senior Lecturer, Robert Gordon University, UK for giving their valuable time and observing the process of the study and giving us directions and recommendations.

Finally, I am also grateful to Dr. Mohammed Mahbubur Rahman, Professor and Head, Department of Petroleum & Mineral Resources Engineering, Bangladesh University of Engineering and Technology for his advice and inspiration.

Table of Contents

LIST OF FIGURES

LIST OF TABLES

NOMENCLATURE

Symbol	Definition	Unit
Roman		
A	Cross-sectional area of the pipe	[m^2]
A_g	Cross-sectional area of the gas phase	[m^2]
A_l	Cross-sectional area of the liquid phase	[m^2]
D	Pipe diameter	[m]
D_{hk}	Hydraulic diameter of phase k	[m]
dp/dx	Pressure gradient	[$Pa.m^{-1}$]
f_k	Wall friction factor of phase k	-
g	Gravitational acceleration constant	[$m.s^{-2}$]
P	Common pressure	[Pa]
P_k	Pressure of phase k	[Pa]
R	Cross sectional pipe radius	[m]
Re_k	Reynolds number of phase k	-
Re_g	Reynolds number of the gas phase	-
Re_l	Reynolds number of the liquid phase	-
Re_m	Reynolds number of the gas-liquid mixture	-
V_g	Gas phase velocity	[$m.s^{-1}$]
V_l	Liquid phase velocity	[$m.s^{-1}$]
V_m	Mixture phase velocity	[$m.s^{-1}$]
Greek		
α_k	Volume fraction or holdup of phase k	-
α_g	Volume fraction or holdup of the gas phase	-
α_l	Volume fraction or holdup of the liquid phase	-
$\Delta\rho$	Density difference	[$kg.m^{-3}$]
ρ_k	Density of phase k	[$kg.m^{-3}$]
ρ_g	Density of the gas phase	[$kg.m^{-3}$]
ρ_l	Density of the liquid phase	[$kg.m^{-3}$]
ρ_m	Density of the gas-liquid mixture	[$kg.m^{-3}$]
μ_k	Viscosity of phase k	[kg/(m.s)]
μ_g	Viscosity of the gas phase	[kg/(m.s)]

μ_l	Viscosity of the liquid phase	[kg/(m.s)]
μ_k	Viscosity of the gas-liquid mixture	[kg/(m.s)]

Abbreviations

CFD	Computational Fluid Dynamics
DNS	Direct Numerical Solution
FMV	Finite Volume Method
GVF	Gas Volume Fraction
VOF	Volume of Fluid

Subscripts

g	Gas phase
l	Liquid phase
m	Mixture gas-liquid

CHAPTER 1
INTRODUCTION

Transportation of cuttings and efficiency of hole cleaning has been one of the major concerns of stake holders in the oil and gas industry. This is because a successful drilling program is a key to a productive and profitable oil and gas business. A successful drilling program is because of an efficiently cleaned hole. On the other hand, a poor or inefficient hole cleaning implies accumulation of cuttings or formation of cuttings bed in the well. This often leads to decreased rate of penetration, increased cost of drilling, fractured formation, increased plastic viscosity of mud because of grinding of cuttings and stuck pipe.

In deviated wells, the transportation mechanism of cuttings seems quite difficult. This trouble emerges from the tendency of cuttings to accumulate in annular bends shown in Fig 1.1. It was found in the literature that cuttings deposition increases in inclined section of annulus contrasted with different areas of the flow stream. This condition is caused by the gravitational force, which helps the solid particles to be stored at the base of the annular area. Test and numerical investigations have indicated that cuttings transport is influenced by numerous parameters. Deviated wells, for the most part, incorporate eccentric state of drill pipe inside the casing, causing stuck channel. The eccentricity of drill string can be characterized as the tendency of drill pipe getting off-centered from casing.

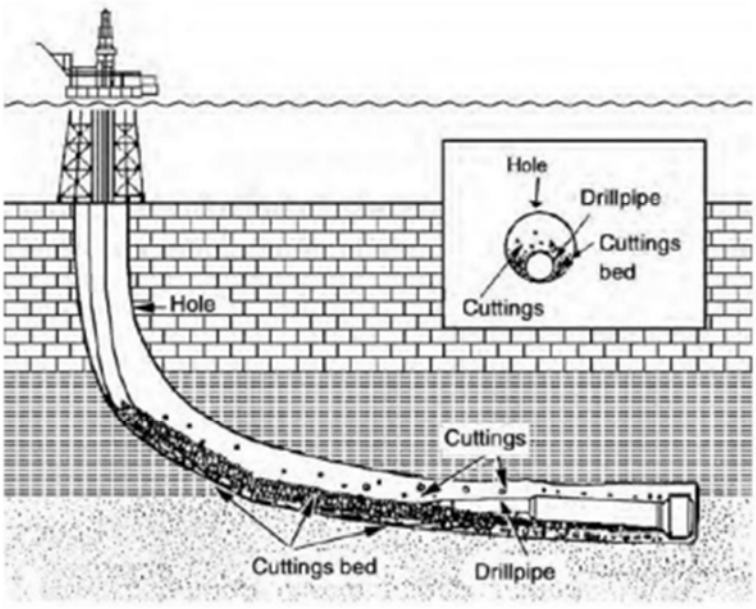

Figure 1.1: Schematic of cuttings bed build-up during directional drilling (Demiralp, 2014)

The bend angle involved in highly deviated wells forces cuttings to form cuttings bed that increases the equivalent circulation density (ECD). It reduces the flow rate of drilling mud and thus cuttings accumulate faster causing wellbore instability, severe mud loss and stuck pipe. This issue may cause genuine difficulty in well and, for some situations, can prompt costly operational problems. Thus, the increasing demand for cutting transport efficiency during the pre-operational phase of a field emerges from economical contemplations and the expanding application of deviated, extended reach and horizontal wells. In such case, rheological properties and pipe rotation are generally optimized to mitigate the effect of hole eccentricity and the bend angle. Therefore, drill pipe drags more fluid, hauling cutting beds with increased velocities leading to higher cutting transport efficiency.

1.1 Scope of the Study

The prime motivation of the study is to design a better cutting transportation system under the eccentric condition of drill pipe and optimize the challenges for directional wells. The study includes modifying the rotational speed of drill pipe involving smaller cutting size carried out by drilling mud, a non-Newtonian fluid. The volume fraction and pressure drop for different annular geometry and rotation of the drill pipe are reported using CFD with the aid of ANSYS FLUENT. It will help to provide a better understanding of the behavior of drill cuttings and insight of cutting transport efficiency for deviated annular geometry and different drilling parameters, which is a significant inefficient design and optimization of drilling operation besides the rheological improvement of drilling mud.

1.2 Objectives

The objectives are:

- Understand the effect of the rotational speed and eccentricity of drill string with multiphase flow model using CFD.
- For Steady State: Study the relation between pressure drops at different RPM with different eccentricity and study the effect of bend angle.
- Proposed appropriate flow equations.
- Find out the optimum conditions for pipeline design.

1.3 Methodology

- Measure the eccentricity.
- Study the pressure and velocity contours.
- Comparison of Volume of fraction at bend-1 (plane-4) for different eccentricity.
- Determine the flow equations of mud circulation using regression analysis.
- Validate the simulations results with previous project.
- From literature find appropriate data to be used in the study.
- Setup simulation model in CFD software.

1.4 Project Outline

In chapter 1, provides a general introduction.

In chapter 2, discusses the previous works and theories related to the study.

In chapter 3, the equations which has been used for our experiment.

In chapter 4, the simulation methodology is described with geometry details, the meshing, boundary conditions and the solution method.

In chapter 5, CFD analysis of pressure drop and all the figures are given which can give a visual perception on our project and the results are also discussed with different graph and result validation.

Chapter 6, discussed the result and conclusion part.

Chapter 7, discussed the relevance and showed a guideline for the future progress.

CHAPTER 2
LITERATURE REVIEW

For CFD modelling and simulation, detail literature reviewed about the simulation, pipeline design parameters, fluid properties, effect of bend angle and eccentricity, pressure drop calculation method etc are required to get the best fitted result.

2.1 Transportation of cutting to the Surface

Cuttings transport efficiency is a measure of the extent to which cuttings are carried to the surface from a drilled hole. It quantifies the success achieved in freeing a well of drilled cuttings. It is also related to the carrying capacity of a drilling mud.

Two of the major concerns in hole cleaning operation are ensuring that the mud has the right capabilities to clean and transport cuttings from the annulus to the surface and ensuring best drilling practices are always implemented.

The first part implies that the drilling mud must have the right rheology for efficient transportation of cuttings to the surface. Methods and models for wellbore cleaning varies for different hole angle of inclination. In hole cleaning process, the wellbore can be divided into 3 sections: low inclination (>30°), Medium inclination (30°-65°) and high inclination (>65°) section.

2.2 Review of factors affecting hole cleaning

Factors affecting hole cleaning can be divided into 3 groups. The first group consists of fluid parameters which include; fluid viscosity, fluid density, and fluid flow rate. The second group consists of cuttings parameters which include; cutting density, size and shape, and cutting concentration in the annulus. The third group consists of pipe rotation, and eccentricity in the hole *(Belavadi & Chukwu, 1994)*. Adari et al., (2010), listed some of the elements affecting hole cleaning, by ranking them based on its importance and influence on hole cleaning, presented in Fig. 2.1.

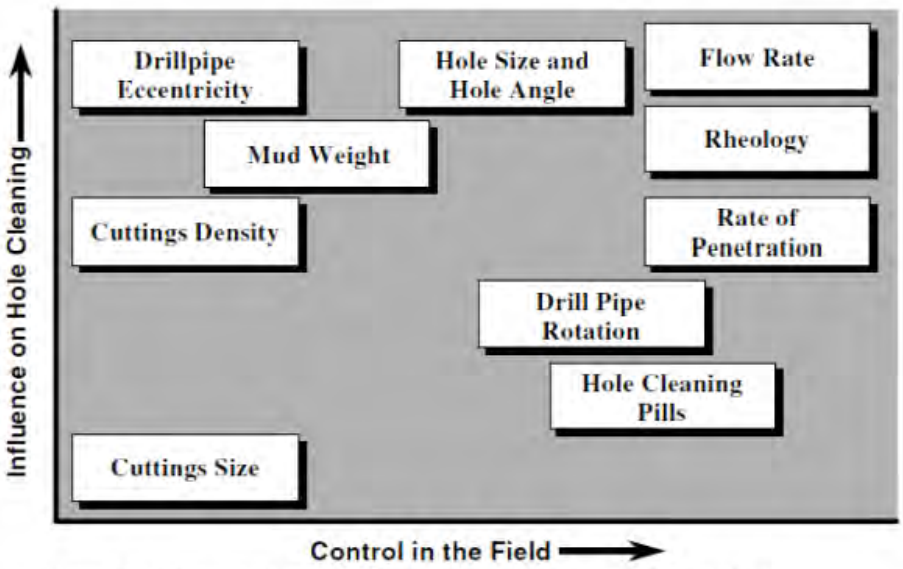

Figure 2.1: Key variables controlling cuttings transport (*Adari et al., 2000*)

Pipe rotation (RPM)

Pipe rotation is known to help significantly improve hole cleaning. The effect of RPM is more noticeable in deviated holes. *Sanchez et al., (1999)* revealed that pipe rotation has significant effect on hole cleaning in directional well. It was observed that a low flow rate with high RPM significantly improved hole cleaning in horizontal wells The Authors stated that smaller cuttings were more difficult to remove from wellbore. However, with a high RPM and high viscosity of mud, it was easier to transport smaller cuttings to surface.

Eccentricity

Effect of eccentricity has been investigated by various authors. Eccentricity is usually prominent in highly deviated wells. In the inclined section of the well, the pipe tends to rest on the low side of the wellbore as a result of gravity. This phenomenon creates a narrow gap between the pipe and the annulus on the low side of the well, thereby causing restriction to the flow velocity of the mud. Iyolo and Azar (1981) revealed the effect of eccentricity on hole cleaning, as they observed low annular velocity at low side of the drill pipe as result of eccentricity. The drilling fluid profile in laminar flow regime created by the eccentricity of drill pipe, affects the efficiency of wellbore cleaning. The effect of drill string sagging at low side of the well, leads to increase in cutting bed height, due to obstruction on annular velocity on the low side of the well.

Rate of penetration (ROP)

Increase in ROP tends to increase or generate more cuttings which adversely affects hole cleaning. The more the cuttings, the higher the required hydraulic output required for efficient hole cleaning. When ROP is high, it is recommended to adjust flow rate and/or RPM for good

hole cleaning. When the effect of flow rate and RPM is exhausted, it is recommended to reduce ROP. Though reduction in ROP can lead to drilling cost, the benefits of avoiding drilling/hole cleaning issues such as mechanical sticking and stuck pipe, outweighs the loss in ROP.

Mud Weight

The two major fluid parameters affecting hole cleaning are mud weight and viscosity. The mud weight primarily provides mechanical borehole stabilization and prevention of invasion of formation fluid into the annulus. In hole cleaning, drilling fluid mud weight has little or no effect on hole cleaning. However, a small increase in mud density decreases bed height (Nazari et al.,2010). Increasing drilling fluid density with same rheology has little or no effect on hole cleaning. Any unnecessary increase in mud weight could lead to formation fracture.

2.3 Two Phase Flow

Singh and Griffith (1970) worked on pipe size and pressure drop in an inclined pipe for two phase slug flow. A model of two phase slug flow was introduced in inclined pipes where the parameters were experimentally determined. Total pressure gradient and the wall shear stress was predicted. The research showed the relation between the size of the pipe and the pressure gradient.

Thomas et al. (1974) researched on two phase flows through curved, vertical, or inclined pipe. A model was predicted for pressure distribution through these pipes which combined the correlation for the pressure gradients for each flow regime. Evaluating the field data and literature data, a procedure was described for generating three-dimensional graph of pressure gradient and holdups.

Masayuki Toda and Hirotaka Konno (1987) researched on modeling and experimental studies the fundamental characteristics of three phase flow of gas-liquid-solid.

Barnea et al. (1986) investigated on flow pattern for upward flow and gas-liquid flow in inclined tubes. Flow pattern calculations for upward liquid gas flow in pipes at inclination angles helped mathematical models for vertical and horizontal configurations extend to cover the full range of pipe inclinations which was presented previously.

Skudarnov et al. (2004) performed experiment on slurry transport of five double-species slurries composed of glass beads and water. Pressure gradient and the solid volume fraction were compared. Effect of the particle diameter was also studied. The diameter of the pipe was 23 mm. it is observed that with the increase in the solid particle gives higher pressure gradients for the low velocity and lower drop of pressure for the higher flow velocity.

Kaushal et al. (2005) conducted an experiment in horizontal pipe that has diameter of 54.9 mm on a glass beads of two sizes having standard deviation and mean diameter of 1.15& 125 μm and 1.2 & 440 μm. Flow velocity was 5 m/s and concentration was up to 50% of the overall volume. It was observed that the pressure drop increases with the increase of the concentration for both the slurry flow velocity of 125 μm and 440 μm. The rate of pressure drop is low at the low velocity but pressure drop is lower at the higher velocity.

Verma et al. (2006) have calculated the pressure drop of the fly ash slurry across the horizontal pipe. High concentrated fly ash has been taken. The experimental data analyzed the loss coefficient at the bend and the relative pressure drop. From the study it was concluded that the pressure drop increases with the increase in velocity, loss coefficient at the bend reduces with the increase of the velocity for the fly ash slurry.

Adel. Salem at el 2007 Worked on simulation and modeling of slug flow and two phase flow characteristics using CFD in inclined and horizontal pipelines. The study investigated the flow characteristics of liquid gas slug using 3D and 2D CFD tools. For the flow pattern of the slurry a set of simulation was run. Two sets of simulation was done on horizontal pipe with the dia of 2 inch and for the pipeline with the inclination angles of +6, 0 and -6 degrees. The simulation and experiment studied the pipe inclination effect on flow regime and computed the pressure drop, flow pattern and liquid holdups.

Adel. Salem at el 2008 worked on the simulation on CFD for the two or multiphase flows in inclined and horizontal pipelines. The main aim of this simulation was to gain the detail and deep knowledge on the flow pattern of the multiphase fluid flow which can help to develop a good guideline to improve the pipeline design in future.
M. Czapp, M. Utschick at el July 2007 was conducted several simulation on multiphase flow. The used various equation on this simulation .among those they used VOF model, standard k-turbulence and Navier Stokes model to resolved the slug flow and formation. The main aim of this study was to determine the slug flow of two phase in pipes.

S. Al-lababidi et al. (2009) worked on the measurement of the fraction of gas void in two phase liquid and gas flow. Correlation between Slug velocity, gas void fraction and absolute emission energy was studied in this paper. The study of Dr Md Alamgir Hossain is carried out to understand the turbid particles behavior through pipes and the similar behavior of the solid particle in turbulent field.

Chen et al. (2009) worked on the simulation of the water coal slurries in a horizontal pipe. He used the Euralian multiphase approach with the k epsilon model equation. The validation was done by the concentration profile data and the pressure gradient. Later on it has been validated by the data of pressure gradient taken from the authors experiment.

Eesa et al. (2009) also studied on the numerical analysis. This time he used the Eulerian-Euleriancomputational fluid dynamics (CFD) model. Coarse particle is used in the carrier fluid which is non Newtonian. The simulation was done in the ANSYS CFX. The conclusion of this study was that with the increase of the concentration the pressure drop is also increased.

Ekambara et al. (2009) have conducted and predicted the flow of liquid solid in a horizontal pipeline by using the transient 3D hydrodynamic model. ANSYS CFX software has been used for getting the simulated result of the slurry flow. The simulated and the experimental result indicated the distribution of the particle flow through a pipeline. And the CFD model explained the concentration profile for the slurry particles.

Vlasak et al. (2009) investigated the bottom ash, sand slurry and fluidic ash to study the effect of volumetric composition and the slurry particle composition on the flow behavior of the coarse and fine grained particle.

Yingjie et al. (2009) studied on the change of viscosity of the oil coal slurry under high pressure and the temperature during heating and also the effect of it.

Chandel et al. (2010) studied on the pressure drop and the rheological behavior of the mixture of bottom ash and the fly ash at a ratio of 1:4. Rheological data has been taken in a straight pipeline having dia of 42 mm to predict the pressure drop. The study showed that the pressure drop increases with the increase of the flow velocity.

Lahiri et al. (2010) studied the flow of slurry using CFD to predict the concentration profile. And the simulated data for the 3D simulation has been validated to the data of Kushal et al (2005).

Lu et al. (2010) Discussed the effect of pressure drop and the distribution of the particle size of slurries.in this study the flow pattern of the different size particle with the different velocity has been observed.

Hossain et al. (2011) performed a numerical simulation. The simulation has been done on a horizontal pipe having four loop of four bends to predict the particle deposition through a

horizontal pipe. the study concluded that the maximum concentration of the particle occurred at the bottom of the pipe.

Mazumdar (2011) performed the CFD analysis in water air two phase flow. Pressure drop profile and the characteristics flow behavior has been discussed in this paper.

Vlasak et al. (2011) investigated an experiment on the pressure drop and flow behavior of the different size particle of sand in dense slurry.

Kaushal et al. (2012) investigated the pipeline slurry flow for the fine particle at high concentration. Mixture and Eulerian two phase model has been used. Horizontal pipe with 54.9 mm and the flow velocity was 5 m/s was used. Concentration was up to 50% by the overall volume was taken. The mixture model failed to give data but the Eulerian model gave the both concentration profile and pressure drop data at all concentration and the velocities. Kumar et al (2012) have done the numerical simulation of the horizontal pipeline flow by using k-epsilon equation.

Bandyopadhyay et al. (2013) performed the CFD analysis for the gas non Newtonian and non-Newtonian flow through elbows. For the two phase fluid flow they have used Eulerian- Eulerian approach. The simulated result was verified by the result of previous author's publications. The result shows that for the non-Newtonian liquid flow the the greatest pressure occurs at the outer wall and least at the inner wall and the maximum velocity shifts towards the inner wall.

Capecelatro et al. (2013) investigated a computation of solid liquid flow to a horizontal pipe to predict the complex multiphase flow dynamics below and above the critical velocity of deposition.

Kaushal et al. (2013) simulated numerically the slurry flow through a horizontal pipe. Eulerian two phase model in fluent software has been used. From this study it has been found that at higher velocities the concentration distribution is more uniform.

Nabil et al. (2013) took an attempt to develop a slurry flow model using CFD for better understanding and for better visualizing the behavior of the slurry flow. The study worked on the velocity profile, pressure drop, and concentration profile on various particle size. Eulerian-Eulerian multiphase model along with the standard k epsilon model has been used.at last it was found that the CFD is capable enough to develop a model which can show the behavior of the slurry.

2.4 Rationale for Applying CFD

Computational fluid dynamics or CFD, as is popularly known, are used with the aid of computers to produce flow simulations. CFD numerically requires the application of the fluid dynamics governing laws. The complex set of partial differential equations is solved in a geometric domain divided into small volumes, commonly referred to as a mesh (or grid). CFD helps analysts to model and understand fluid flows at specific locations without the assistance of instruments to calculate various flow variables. Thus CFD has become very popular in oil and gas industry to study the annular transportation efficiency of the drill cuttings as a successful drilling operation greatly depends on the cuttings transportation from the downhole to the surface. Again prediction of annular pressure drop is also a critical factor that helps to optimize pump pressure required or the suitable pump capacity. Studies regarding drilling operation has become easier for CFD studies as the simulated result is consistent with the experimental or real field results.

2.5 CFD Works in this Area

Table-2.1: Summary of previous studies investigating the effect of Drill–pipe rotation on hole cleaning.

Authors	Approach	Remarks
Pang et al. (2018,2019)	CFD	The drill pipe rotation produces a spiral flow, whereas orbital motion of the drill pipe improves cutting transport but increases both the resistance and resultant moment exerted by the liquid-solid mixture.
Ytrehus et al. (2018)	Experimental	Cutting transport in the absence of drill pipe rotation is significantly better when the well angle is less than the critical angle.
Moraveji et al. (2017)	CFD	Drill pipe rotation affects hole cleaning when the inclination is increased
Epelle and Gerogiorgis (2018)	CFD	Pipe rotation accompanied by a slight pressure increase improves hole cleaning.
Heydari et al. (2017)	CFD	Pipe rotation effect is negligible at certain speeds of rotation and may increase cuttings accumulation due to eccentricity
Akhshik et al. (2015)	CFD-DEM	When a critical speed at high fluid inlet velocities is attained, the contribution of drill pipe rotation vanishes.

2.6 Summary of Literature Review

From previous investigation it is found that several parameters like drill pipe rotation speed, drilling mud nature, flow pattern through the annulus, eccentricity, mud circulation rate etc. influences the pressure drop and the cutting accumulation in the annulus. Most the studies are related to the vertical experimental setup and as the interest for directional drilling is increasing and is a popular operation throughout the world, there is still lack of studies regarding directional drilling geometry. Thus, In this project paper the effect of drill pipe rotation, eccentricity and the effect of bend angle change for directional drilling geometry is investigated.

CHAPTER 3
NUMERICAL MODELING

A multiphase flow system consists of several single-phase regions which are bounded by moving interfaces. In principle, a multiphase flow model can be formulated in terms of the local instant variables relating to each phase and matching boundary conditions at all phase interfaces. It is extremely complicate to obtain solution of multiphase system directly or in other words it is almost impossible to solve directly. As a starting point for derivation of macroscopic equations which replace the local instant description of each phase by a collective description of the phases.

For the formulation of the multiphase flow, averaging procedures can be classified into three main groups, the Boltzmann averaging, the Lagrangian averaging and the Eulerian averaging. These groups can be further divided into sub-groups based on the variable with which a mathematical operator or averaging is defined. Here we will discuss about two numerical approaches for solving multiphase flows in CFD. They are:

1. Eulerian – Lagrangian approach
2. Eulerian – Eulerian approach

3.1 Eulerian - Lagragian Approach

This approach is applicable to continuous-dispersed systems and is often referred to as a discrete particle model or particle transport model. The primary phase is continuous and is composed of a gas or a liquid. The secondary phase is discrete and can be composed of particles, drops or bubbles.

In the Eulerian–Lagrangian (*E–L*) approach, the continuous phase is treated in Eulerian framework (using averaged equations). Its continuous-phase flow field is computed by solving the Navier-Stokes equations. The dispersed phase is represented by tracking a small number of representative particle streams. For each particle stream, ordinary differential equations representing mass, momentum and energy transfer are solved to compute its state and location. The two phases are coupled by inclusion of appropriate interaction terms in the continuous-phase equations. In this approach the volume displaced by the dispersed phase is not taken into account. So, this approach is applicable for low-volume fractions of the dispersed phase. This approach is applicable for situations in which the discrete phase is injected as a continuous stream into the continuous phase. A force balance equation based on Newton's second law of motion is solved to compute the trajectory of the discrete phase.

The Eulerian-Lagrangian approach is suitable to unit operations in which the volume fraction of the dispersed phase is small, such in spray dryers, coal and liquid fuel combustion, and some particle-laden flow. This approach provides complete information on the behavior and residence time of individual particles. Interaction of individual particle streams with turbulent eddied and solid surfaces such as walls can be modeled.

3.2 Eulerian – Eulerian Approach

Eulerian-Eulerian approach is the most general approach for solving multiphase flows. Itis based on the principle of interpenetrating continua, where each phase is governed by the Navier-Stokes's equations. The phases share the same volume and penetrate each other in space and exchange mass, momentum and energy. Each phase is described by its physical properties and its own velocity, pressure, concentration and temperature field. The interphase transfer between phases is computed using empirical closure relations. The Eulerian-Eulerian approach is applicable for continuous-dispersed and continuous-continuous systems.

For continuous-dispersed systems, the velocity of each phase is computed using the Navier-Stokes equations. The dispersed phase can be in the form of particles, drops or bubbles. The forces acting on the dispersed phase are modeled using empirical correlations and are included as part of the interphase transfer terms. In addition, drag, lift, gravity, buoyancy and virtual-mass effects are some of the forces that might be acting on the dispersed phase. These forces are computed for an individual particle and then scaled by the local volume fraction to account for multiple particles.

There are three different Euler-Euler multiphase models available:

- Volume of fluid method (VOF)
- Mixture model
- Eulerian model

3.2.1 Volume of Fluid Method (VOF)

In computational fluid dynamics, the Volume of fluid method (VOF) is one of the most well-known methods for volume tracking and locating the free surface. The motion of all phases is modeled by solving a single set of transport equation with appropriate jump boundary conditions at the interface. It can model two or more immiscible fluids by solving a single set of momentum equations and tracking the volume fraction of each of the fluids throughout the domain. Typical applications include the motion of large bubbles in a liquid, the motion of

liquid after a dam break, the prediction of jet breakup, and the steady or transient tracking of any liquid-gas interface.

In general, the steady or transient VOF formulation relies on the fact that two or more fluids (or phases) are not interpenetrating. During the numerical calculation in each control volume, the sum of the volume fractions of all phases remains to unity. In addition, the fields for all properties and variables are shared by the phases and represent volume-averaged values, as long as the volume fraction of each of the phases is known at each location. Thus, in any given cell, the properties and variables are either purely representative of one of the phases, or representative of a mixture of the phases, depending upon the volume fraction values.

3.2.2 Mixture Model

The mixture model is a simplified multiphase model that can be used in different ways. The mixture model can apply to model multiphase flows where the different phases move at different velocities and also it is applicable to model homogeneous multiphase flow and to calculate non-Newtonian viscosity.

The mixture model can model *n* phases (fluid or particulate) by solving both the continuity equation and the momentum equation for the mixture, where mixture can be a combination of continuous phase and the dispersed phase. In addition, the mixture model solves the energy equation for the mixture and the volume fraction equation for the secondary phases, as well as algebraic expressions for the relative velocities (if the phases are moving at different velocities). Also it allows us to select the granular phases and we can calculate the different properties for granular phases. It is applicable in the particle-laden flows with low loading, and bubbly flows where the gas volume fraction remains low, cyclone separators, sedimentation and in liquid-solid flows.

3.2.3. Eulerian Model

Eulerian model is the most general model for solving multiphase flows. In the present work, we are using Eulerian model to simulate two-phase and three-phase flow. The Eulerian model is the most complex of the multiphase models.

Multiphase Model

The Eulerian model based on the Euler–Euler approach is used in the present CFD study as the multiphase model (Fluent 2021 R1). This is because this investigation includes solid liquid two-

phase flows, in which both granular (fluid–solid) and nongranular (fluid–fluid) flows are involved. The Eulerian model is known to be capable of addressing different kinds of couplings with individual momentum and continuity equations quite effectively.

Volume of Fractions

Volume fractions represent the space occupied by each phase, and the laws of conservation of mass and momentum are satisfied by each phase individually. The conservation equations can be derived by averaging the local instantaneous balance for each of the phases or by using the mixture theory approach. The volume fraction of each phase is calculated from the continuity equation.

Eccentricity Calculation

Based on Schlumberger Oilfield Glossary, eccentricity is described as how much offset a pipe is within another pipe or in the open hole and usually expressed in term of percentage (%). If the inner pipe is perfectly centered within the outer pipe, the inner pipe is said to be concentric. And if the inner pipe is lying close to the outer pipe and has an offset from the center, the inner pipe is considered eccentric. However, if the inner pipe touches or in contact with the wall of outer pipe, the condition is said to be fully eccentric (100 % eccentric).

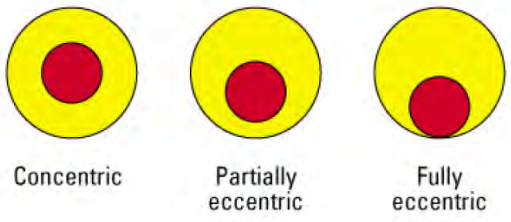

Figure 3.1: Diagram of type of eccentricity.

The offset of the inner pipe from center will be determine by using formula below.

$$e = \frac{2\delta}{d_2 - d_1}$$

where, e = eccentricity

δ = distance of offset from center

$d1$ = diameter of the inner pipe

$d2$ = diameter of the outer pipe

CHAPTER 4
METHODOLOGY

This project involves CFD modelling of drill cuttings transportation through annular bends. Specify the inlet boundary conditions and calculate the corresponding pressure and VOF at various sets of inputs. This chapter outlines the methodology for the execution of the project.

4.1 CFD Methodology

The complete CFD analysis procedure can be divided into the following six stages:

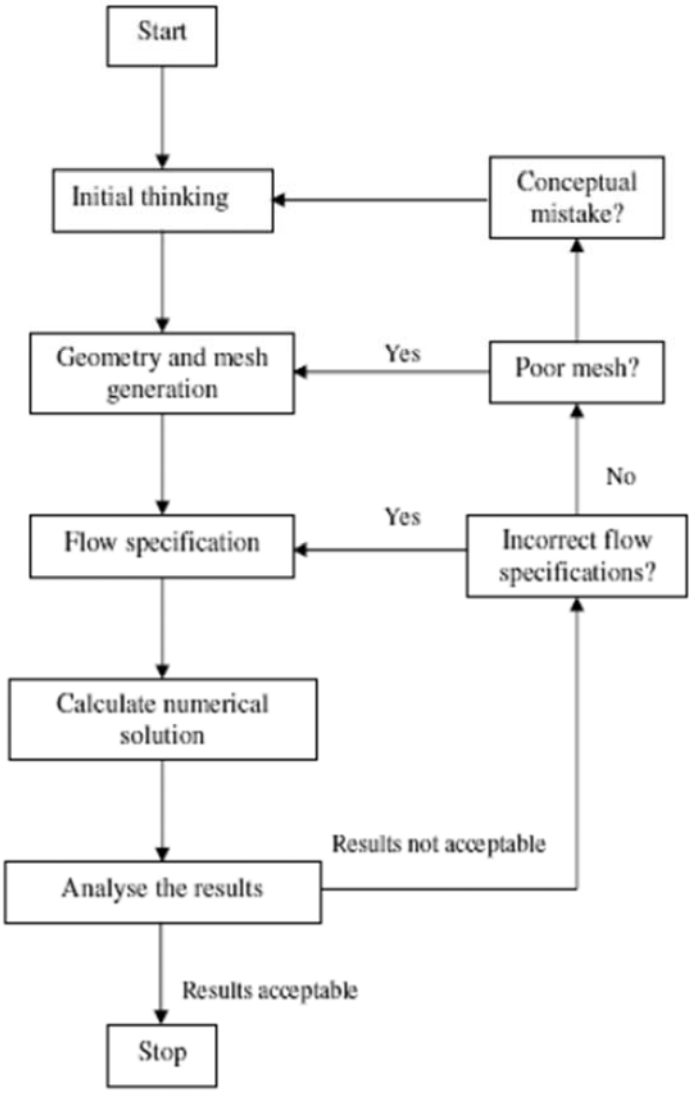

For mathematical modelling of a flowing fluid through a pipe there are three steps that are followed.

- Developing the flow-specific governing equations.
- Discretization of the governing equations.
- Solving the mathematical equations that arise.

4.2 Model Equations

The local shear stresses and the local shear rate in the fluid have a non-linear relationship in a non-Newtonian fluid where a constant of proportionality cannot be defined. Therefore, 'Viscosity ' is a variable, not a fixed scalar. Further it is also important to note that the viscosity can be dependent on the shear rate or the time history of shear rate.

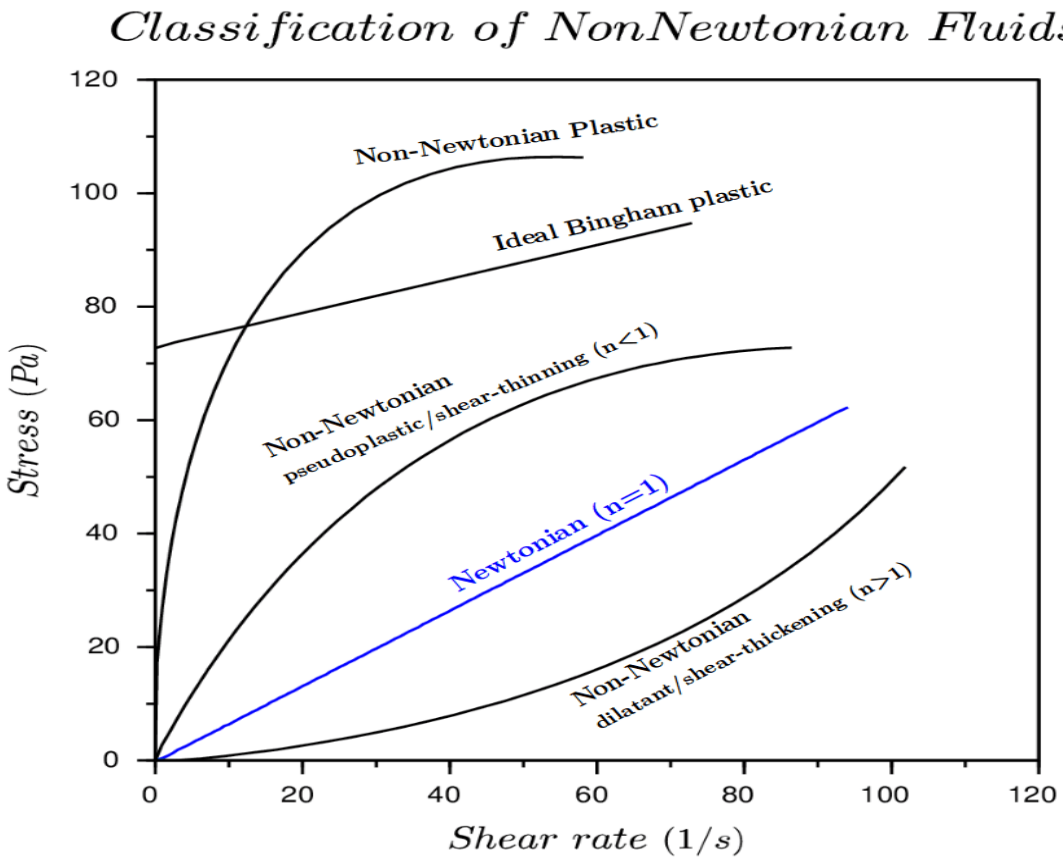

Figure 4.1: A typical stress-strain plot for Non-Newtonian fluids (SimScale, 2021).

4.2.1 Power Law Model

A ' Power-Law ' model of fluid is a generalized non-Newtonian model of fluid. It gives a basic relation for viscosity ν, and the strain rate γ. In this model, the value of viscosity can be bounded by a lower bound value, Vmin, and a upper bound value Vmax.

The relation is given as:

$$v = k\dot{\gamma}^{n-1}$$

Where,
K is the flow consistency index (SI units m^2/s),
$\dot{\gamma}$ is the strain-rate (SI units s^{-1}),
n is the flow behavior index.

Based on the flow behavior index, n:

- If 0<n<1: The fluid shows 'Pseudo plastic or Shear thinning' behavior. Here a smaller
- value of n, means a greater degree of shear-thinning.
- If n=1: The fluid shows Newtonian behavior
- If 1<n: The fluid shows 'Dilatant or shear thickening' behavior with higher value
- of n resulting in greater thickening.

4.2.2 Herschel-Bulkley Model

The fluid ' Herschel – Bulkley ' is also a common, non-linear model of non-Newtonian fluids. This model combines the behavior of Bingham and power-law fluids in a single relation. For very low strain rates, the material behaves as a very viscous fluid with viscosity v_0. After a minimum value of strain-rate corresponding to a threshold stress τ_0, the viscosity is represented by the power law relation.

The model formulation is given as:

$$v = \min(v_o, \frac{\tau_o}{\dot{\gamma}} + k\dot{\gamma}^{n-1})$$

Where,

n is the 'Power/Flow Index'

k is the 'Consistency Index' with units m^2/s

τ_o is the yield stress

v_o is the viscosity at zero shear rate.

Further, if $\tau > \tau_o$ the Herschel-Bulkley fluid behaves as a fluid.

- if 0<n<1: The fluid shows 'Pseudo plastic or Shear thinning' behavior.
- if n=1 and τ_o=1: The fluid shows Newtonian behavior
- if 1<n: The fluid shows 'Dilatant or shear thickening' behavior.

Power Law is the simplest model that approximates the behavior of a non-Newtonian fluid. The limitation is that it is only true for a limited range of shear rates. Therefore the values of k and n are dependent on the range of shear rates taken into account. That is why in this research work for the purpose of considering a non-Newtonian conveying medium Herschel-Bulkley model is adopted.

4.2.3 Equations Describing Fluids in Motion

For explaining fluid flow the mathematical equations that are used-the equations of continuity and momentum which describe mass and momentum conservation respectively. Often known

as the Navier-Stokes equations, the momentum equations. For flows involving heat transfer, the definition of energy conservation includes another set of equations.

Continuity equation measures the volume fraction of each phase:

$$\frac{1}{\rho_{rs}}\left(\frac{\partial}{\partial t}(\alpha_s\rho_s) + (\alpha_s\rho_s\vec{v}_s) = \sum_{l=1}^{n}(\dot{m}_{ls} - \dot{m}_{sl})\right) \quad (1)$$

Fluid-solid momentum equation:

$$\frac{\partial}{\partial t}(\alpha_s\rho_s\vec{v}_s) + (\alpha_s\rho_s\vec{v}_s\vec{v}_s) = -\alpha_s\nabla p - \nabla p_s + \nabla.\bar{\bar{\tau}}_q + \alpha_s\rho_s\vec{g} + \sum_{l=1}^{N}(k_{ls}(\vec{v}_l - \vec{v}_s) + \dot{m}_{ls}\vec{v}_{ls} - \dot{m}_{sl}\vec{v}_{sl}) + (\vec{F}_s + \vec{F}_{lift,s} + \vec{F}_{vm,s} + \vec{F}_{td,s}) \quad (2)$$

Where $\vec{v}_s$ is the velocity of the solid phase, $\vec{v}_l$ is the velocity of the liquid phase, αs is the volume fraction of the solid phase, ρ_s is the density of the solid phase, ρ_l is the liquid phase density, $\dot{m}_{ls}$ and $\dot{m}_{sl}$ characterize the mass transfer between solid and liquid phases respectively, $\vec{v}_{ls}$ and $\vec{v}_{sl}$ are the interphase velocities, g is the acceleration due to gravity, ρ_{rs} is the phase reference density, $\vec{F}_s$ is an external body force, $\vec{F}_{lift,s}$ is the lift force, $\vec{F}_{vm,s}$ is the virtual mass force and $\vec{F}_{td,s}$ is the turbulent dispersion force (applicable to turbulent flows only). The equation for the force terms are detailed in the Fluent theory manual (2017). Depending on the prevalent flow regime and transport phenomena, some terms (such as the turbulent dispersion force $\vec{F}_{td,s}$ and mass transfer terms, $\dot{m}_{ls}$ and $\dot{m}_{sl}$) of the Eq. 2 become redundant. Hence, the equation looks like:

$$\frac{\partial}{\partial t}(\alpha_s\rho_s\vec{v}_s) + \nabla(\alpha_s\rho_s\vec{v}_s\vec{v}_s) = -\alpha_s\nabla p - \nabla p_s + \nabla.\bar{\bar{\tau}}_q + \alpha_s\rho_s\vec{g} + \sum_{l=1}^{N}(k_{ls}(\vec{v}_l - \vec{v}_s) + (\vec{F}_s + \vec{F}_{lift,s} + \vec{F}_{vm,s}) \quad (3)$$

4.3 Assumptions:

- Particles and the non-Newtonian fluid (which is the conveying medium) are considered to be continuous.
- No-slip condition between continuous phases and the walls (drill pipe and wellbore).
- Particle shape factor is not included.
- According to particle-particle interactions, there is no form or mass change.
- The casing inner wall and the drill pipe outer wall is assumed to be smooth (there is no roughness factor).
- Initial volume fraction of the cuttings is considered 0.1 .
- For the multiphase flow implicit solution is considered for steady state condition.
- Particle inlet velocity is assumed to be 0.5 m/s.
- A velocity inlet and atmospheric pressure outlet is adopted for the simulations in this project.

4.4 Computational Domain and Physical Parameters

The computational domain consists of a wellbore segment of 2.34m. The geometry of the domain and the mud properties are similar to the work of Epelle, Gerogiorgis (2018). Table-4.1: Physical dimensions of the CFD domain and different parameters are given below-

Physical Parameters	
Particulars	**Drilling Mud**
Geometry	
Drill Pipe Diameter, dpipe (m)	0.113
Wellbore Diameter, dwb (m)	0.18
Computational Length, (m)	2.34
Particle Parameters	
Cutting's material	Sulfur-Solid
Cuttings Density, ρs (kg.m-3)	2800
Viscosity (Kg/m-s)	1.72E-05
Fluid material	Water-Liquid
Cuttings Diameter (m)	0.008
Fluid Density, ρs (kg.m-3)	1000
Viscosity (Kg/m-s)	0.00553
Drilling Variables	
Fluid Inlet Velocity, Vl (m/s)	0.8
Cuttings Inlet Velocity, Vs (m.s-1)	0.5
Drill Pipe Rotation, rpm	0,50,100,150,200
Hole Eccentricity, e	0,0.2,0.4,0.6
Initial Cutting Volume Fraction	0.1

4.5 Numerical Procedure

The governing equation is solved to investigate the flow of Herschel-Bulkley fluid flow through an annular trajectory using a finite-volume computational fluid dynamics (CFD) method. The pressure term in the governing equations has been discretized by second-order upwind scheme and the momentum term by the second order upwind scheme as well. For pressure-velocity coupling, the Semi Implicit Method for Pressure Linked Equations (SIMPLE) algorithm has been used. The SIMPLE algorithm was commonly used in CFD analysis to solve the Navier-Stokes equations numerically.

4.6 Solution Steps and Mesh Size

Using the integrated meshing program in ANSYS as shown in next chapters the computational domain was discretized. Since the computational domain has a complex bent annular geometry with certain angles a Hexahedral Meshing is adopted. Smaller grid size increases the number of total nodes and total elements along the computational domain which can produce more accurate results but will take more computational time and more sophisticated computer capacity. The optimized mesh is used to simulate the HBL type of drilling fluid flow through the annular gap between the drill hole and the drill pipe numerically based on the results of the analysis. Each of the simulation runs had to converge around 1,000 iterations. The time needed for each run was about 0.5-2.61 hours.

CHAPTER 5
CFD ANALYSIS OF PRESSURE DROP

Introduction

Computational Fluid Dynamics (CFD) is an engineering tool that is used to predict the flow behavior of different types of fluid by numerical simulations. The capacity of CFD displaying is ceaselessly developing as individuals apply this integral asset for various kinds of flowing fluid streams. In this project, the CFD study of the multiphase flow through the drill pipe annular trajectory is studied and the efficiency of cutting transportation along with the drill cutting volume fraction accumulation is analyzed through CFD simulation. This chapter contains the CFD analysis of pressure drop through the annular drill pipe section is analyzed as a function of drill pipe rotating change.

5.1 Approach

At first step of evaluation of the effect of the drill pipe rotation on the pressure drop along the annuli, it is decided to perform 3D simulation of a concentric pipe using four different RPM and evaluate the effect in pressure drop.

The next step is the 3D simulation of an eccentric pipe using the previous five RPM and evaluates the effect in the pressure change as well as pressure drop. It completes the photos of the whole computational study and gives a likelihood to make by and large decisions about the acceptability of the project.

5.2 Assumptions and Uncertainties

When we think about the CFD simulation, it is important to refer to the assumptions and uncertainties which may have an impact on the outcomes of the project. These assumptions and uncertainties present in every one of the reproductions of all the simulation stages, some of the related ones are therefore mentioned in this piece of the report.

Assumptions:

- Single-phase fluid water liquid was considered.
- No heat transfer is included.
- Pipe walls have zero hydraulic roughness.

Uncertainties:

- The dimension of the pipe

  There is a possibility that the initiated rig dimensions might be slightly different from the simulated ones due to the limitation of the simulated measurements as well as the design modeling process.

- Fluid properties

  The fluid properties used in the simulation might be slightly different from the experimental ones. The fluid properties offered by default ANSYS Fluent settings are used in the simulation.

5.3 3D Simulation of Concentric Pipe

5.3.1 Geometry

For all the simulations in this thesis paper Geometry is created in ANSYS Design Modular. This apparatus is sufficient to make basic pipe geometries as well as the complex ones. The geometry for the 3D simulations of the bend pipe is shown in Figure 5.1.

The entire pipe is created in a single body. This is made to easily use the Sweep method to create the inner drill pipe.

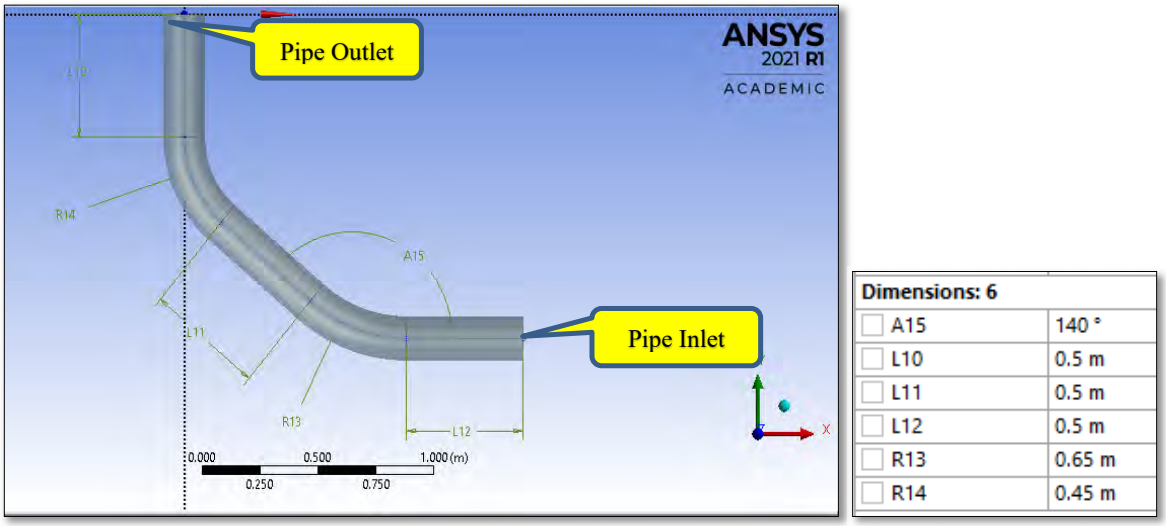

Figure 5.1: Geometry of deviated well

5.3.2 Table-5.1: Model Setup for concentric condition

Preliminary Model Setup for concentric condition	
Inhomogeneous Models	Eulerian
Eulerian Parameter	Multi-Fluid VOF Model
Volume Fraction Parameters	Implicit
Interface Modeling	Sharp/Dispersed
Parameter	**Model/Value**
Model	Realizable k-ε Model
Near Wall Treatment	Enhanced Wall Treatment
C2-Epsilon	1.9
C3-Epsilon	1.3
TKE Prandtl Number	1
TDR Prandtl Number	1.2
Dispersion Prandtl Number	0.75

5.3.3 Mesh

All the required mesh for this research is generated using the ANSYS Meshing tool. Below figures represents all the mesh for different test cases. The mesh statistics and all other important parameters are shown below.

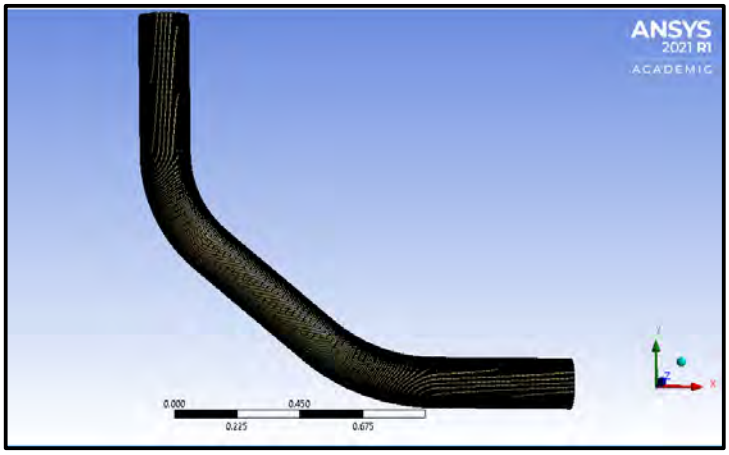

Figure 5.2: Geometry (length)

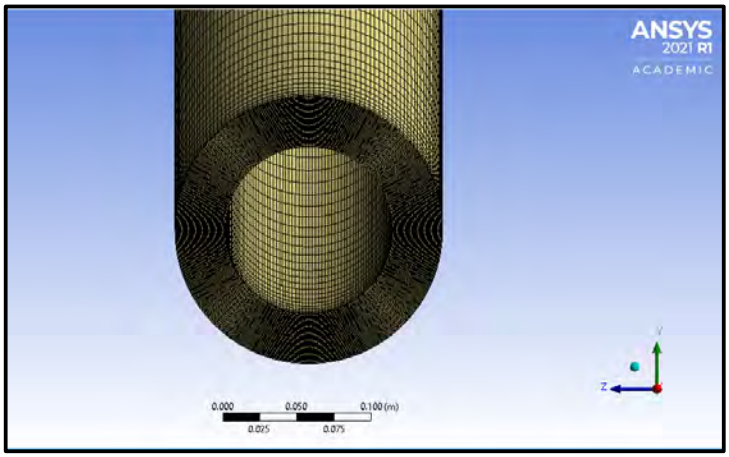

Figure 5.3: Front

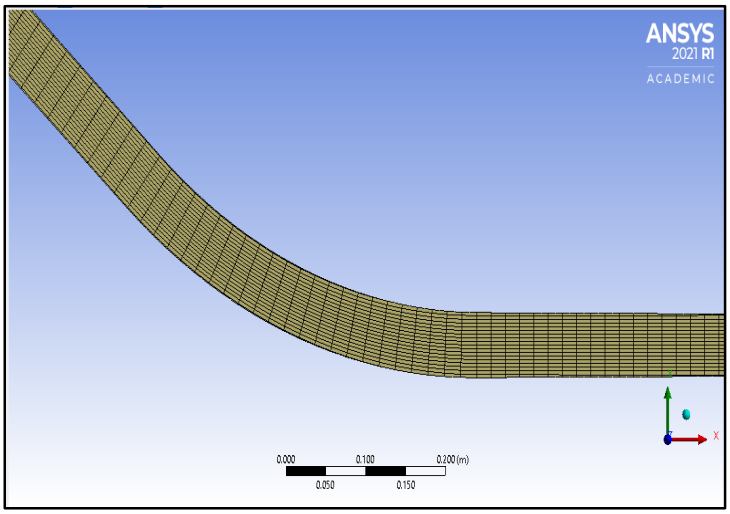

Figure 5.4: Meshing of the deviated pipeline (cross section)

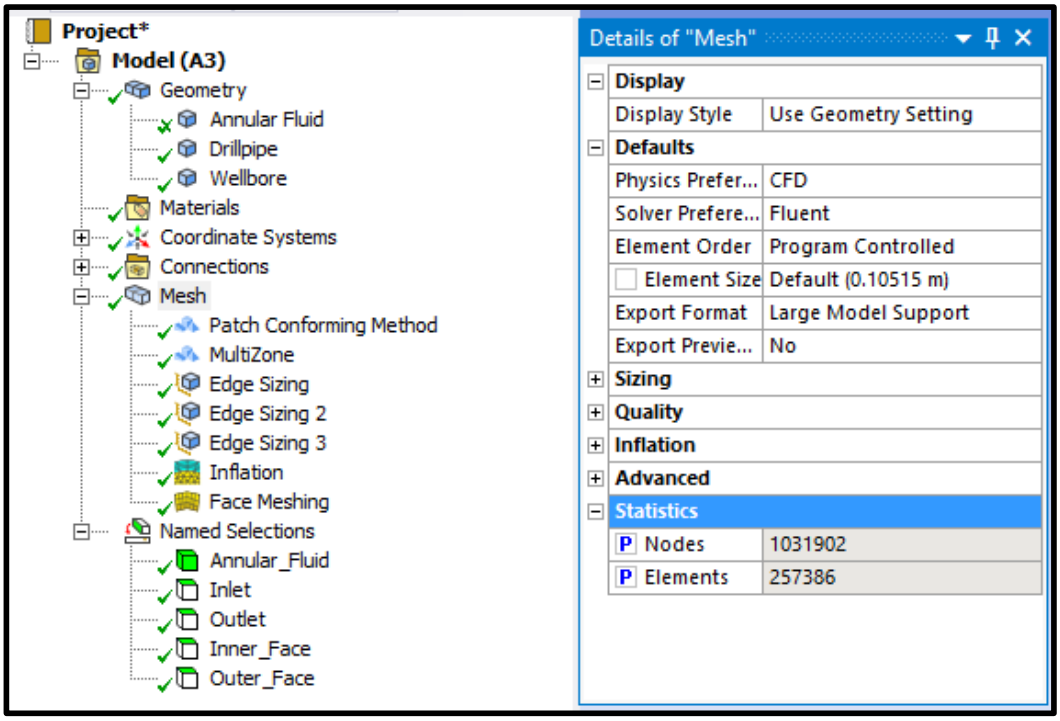

Figure 5.5: Meshing Nodes & Elements

The mesh profile created by MultiZone method, this method can select multiple faces automatically and create hexahedral mesh through out the length. Through this method its easier to indicate the annular liquid and cuttings flow from inlet to outlet by Inflation method. Edge sizing means divide the annular fluid inlet and outlet portion with equal number of division. Edge sizing and Patch Conforming Method are pre-requisite to run the MultiZone Method and Inflation. Finally the number mesh element become 2,57,386 for the simulated model.

5.4 Boundary Condition and Solver Settings

Below boundary conditions and Phase Properties considered for eccentricity 0, 0.2, 0.4, 0.6 .

Table-5.2: Phase Properties for all 3D simulation

Phase Properties	
Fluid Density, ρs (kg.m-3)	1000
Cuttings Density, ρs (kg.m-3)	2800
Cuttings Viscosity (Kg/m-s)	0.001003

Table-5.3: Boundary Conditions for all 3D simulation

Inlet Boundary Conditions	
Turbulent Intensity, %	5
Fluid Inlet Velocity, Vl (m/s)	0.8
Cutting Inlet Velocity, Vs (m/s)	0.5
Initial Gauge Pressure, Pa	0
Outlet Boundary Conditions	
Turbulent Intensity, %	5
Gauge Pressure, Pa	0
Casing	
Wall Motion	Stationary Wall
Shear Condition	No-Slip
Drill Pipe	
Case 01:	
Wall Motion	Stationary Wall
Shear Condition	No-Slip
Speed, RPM	0
Case 02:	
Wall Motion	Moving Wall
Motion	Rotational
Shear Condition	No-Slip
Speed, RPM	50
Case 03:	
Wall Motion	Moving Wall
Motion	Rotational
Shear Condition	No-Slip
Speed, RPM	100
Case 04:	
Wall Motion	Moving Wall
Motion	Rotational
Shear Condition	No-Slip
Speed, RPM	150
Case 05:	
Wall Motion	Moving Wall
Motion	Rotational
Shear Condition	No-Slip
Speed, RPM	200

Table-5.4: Solver settings for 3D Simulation

Solver Settings	
Scheme	SIMPLE
Gradient	Least Squared Cell-Based
Momentum	Second-Order Upwind
Pressure	Second-Order Upwind
Turbulent Kinetic Energy	Second-Order Upwind
Turbulent Dissipation Rate	Second-Order Upwind

The simulation is run in Steady State Mode with the gravity force in negative Z-direction. The value of 10^{-7} is chosen as the convergence condition for all residuals.

5.5 Simulation Result

The simulation is carried out in a deviated pipe using Eulerian equation model. The length of the pipe is 2.34 m, wellbore diameter 0.18m and drill pipe diameter .113m, meshing element is more than 2.5 K. This is a multi-phase flow investigation with water& cuttings used as working fluid. With different rpm at different eccentricity identify the pressure, velocity and VOF profile. The water is used as primary fluid and cuttings as secondary.

In this section the effect of pipe eccentricity on frictional pressure drop is analyzed for CFD model for four eccentric conditions (e = 0.2, 0.4, 0.6, 0.8) in the below mentioned plane position

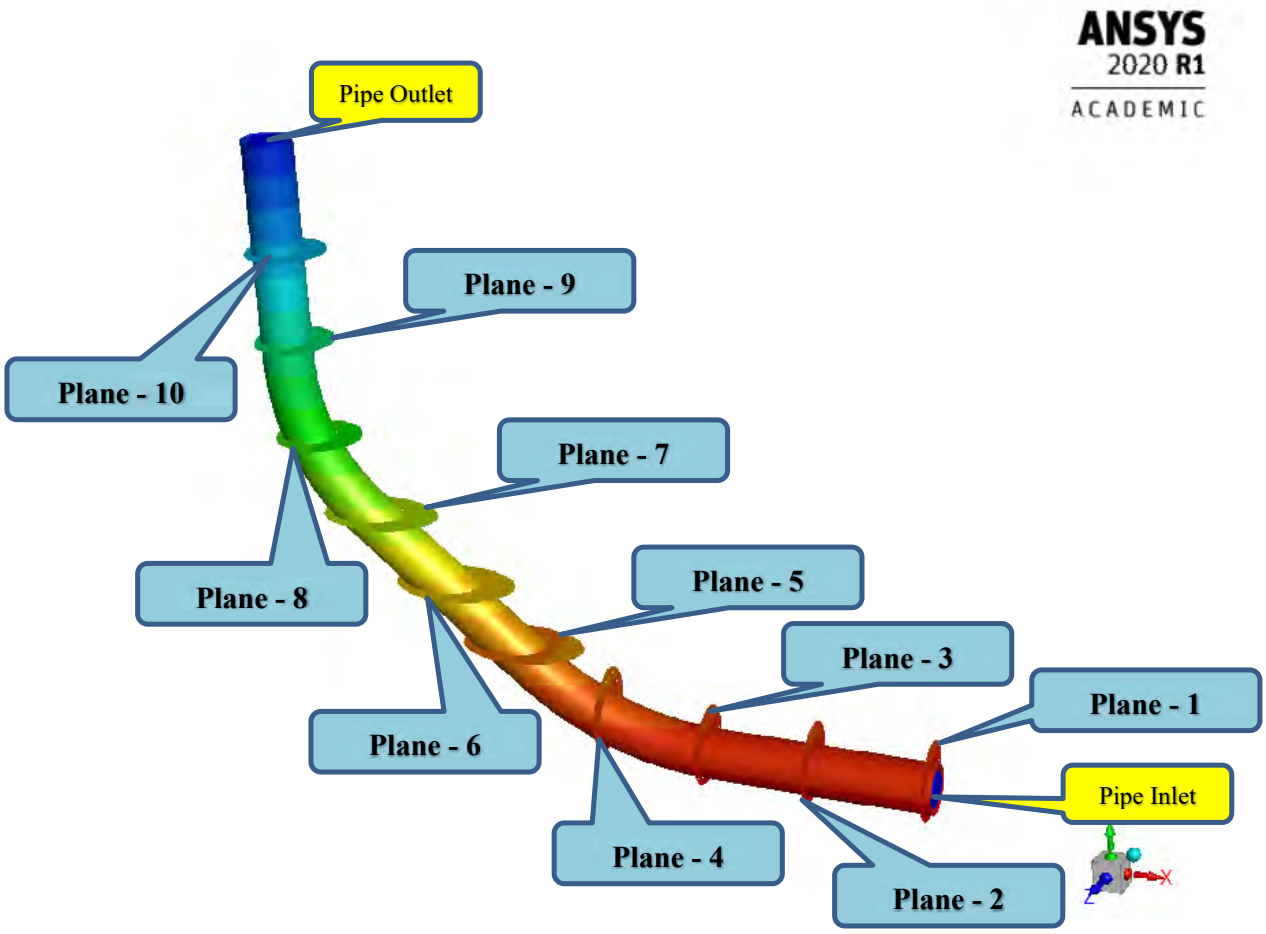

Figure 5.6: Plane Positions in the Bend Pipe Geometry

In the simulated model create plane-1 to 10, to measure pressure in each portion of the pipe. Also, to measure the pressure drop at outlet from inlet and to identify the pressure drop at bends. Each plane helps to identify the pressure drop and VOF, changes with respect to RPM and Eccentricity.

At constant eccentricity, the pressure drop shown with the change of RPM:

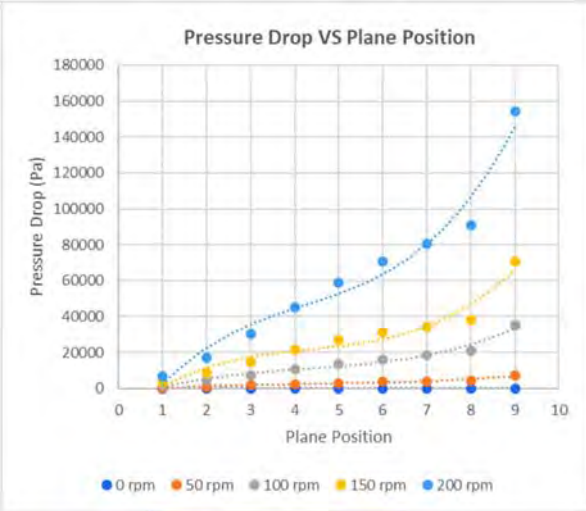

Eccentricity, ε = 0

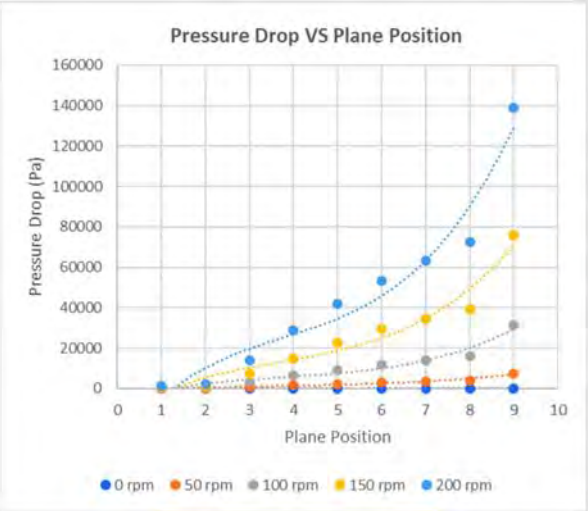

Eccentricity, ε = 0.2

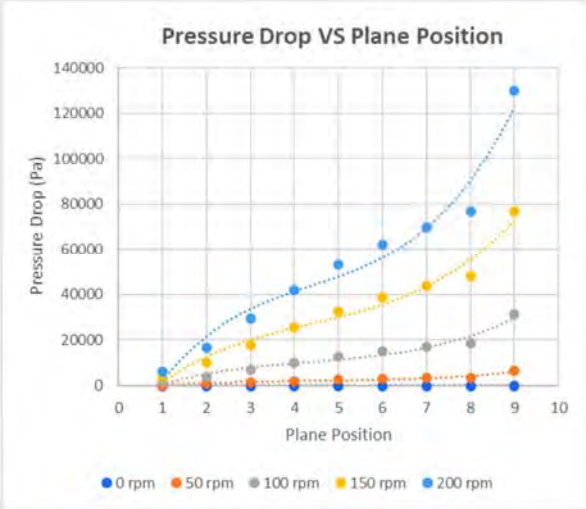

Eccentricity, ε = 0.4

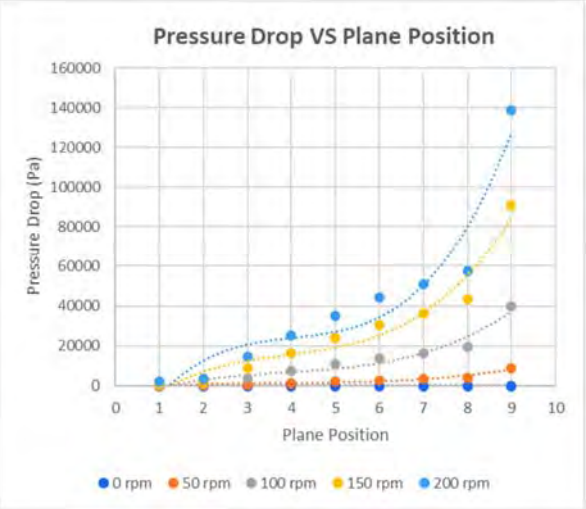

Eccentricity, ε = 0.6

Figure 5.7: Pressure Drop at all Plane Position for different Eccentricity and RPM

Above figures depicts the relationship of pressure drop with the plane position for the different eccentric condition. Pressure drop gradually increases as the fluid advances towards the outlet of the pipe and At Bend-1 pressure drop for planes 1-5 is increasing for five different drill pipe rotation. The values are shown in **Appendix.**

At Bend-2 (plane7-8),

For e =0 pressure drop is 50.87% at 150 RPM and 200 RPM respectively.

For e =0.2 pressure drop is 53.64% at 150 RPM and 200 RPM respectively.

For e =0.4 pressure drop is 39.64% at 150 RPM and 200 RPM respectively.

For e =0.6 pressure drop is 44.41% at 150 RPM and 200 RPM respectively.

Comparison between high pressure planes at bend-1 and bend-2

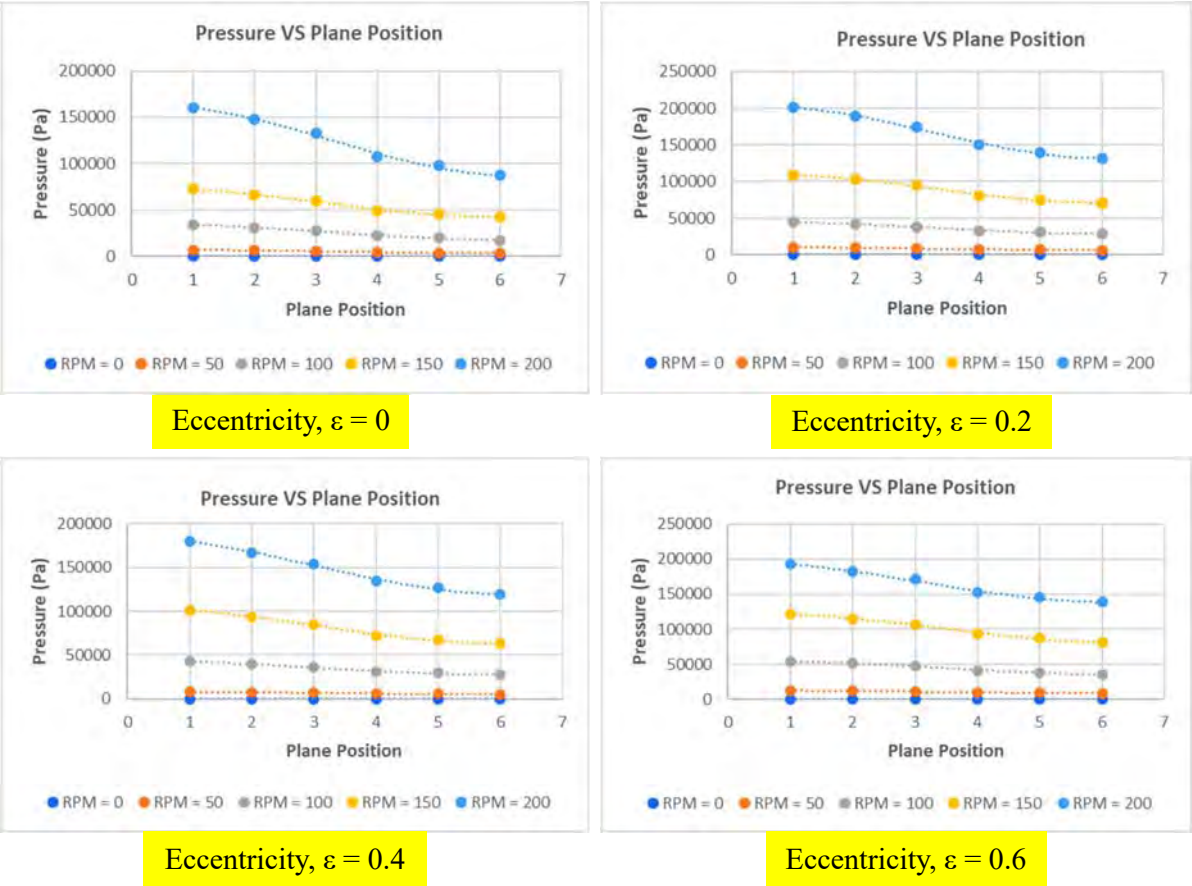

Figure 5.3: Pressure Drop at Bend-1 and Bend-2 for different Eccentricity and RPM

Above figures shows a different scenario at bend-1 and bend-2. Due to the increase in eccentricity, the annular gap has decreased at the lower side of the annulus and the second bend starts in-between planes 7 and 8, therefore, there is a smaller way for the fluid to pass through. Hence the fluid could not pass through the annular gap easily and generates some extra pressure which exceeds the initial pressure. Pressure drop is also increased as drill pipe rotation is increased because of the initial pressure being relatively increasing for the additional drill pipe rotation. As eccentricity has been changed from 0.4 to 0.6 and 0.8 smaller passageway at the annuli makes a hindrance for the fluid to flow and generates some excessive pressure which is again stabilized after the entrance of the second bend.

5.6 Effect of Rotational Speed

The annular pressure drop and volume fractions of cuttings are reported for different eccentricity of drill pipe varying the rotational speed in a range of 0 to 200 rpm to assess the effect of pipe rotation. Result obtained from the analysis shows significant difference in pressure drop volume fractions and velocity in each plane due to the change of rotational speed.

5.6.1 Pressure gradient:

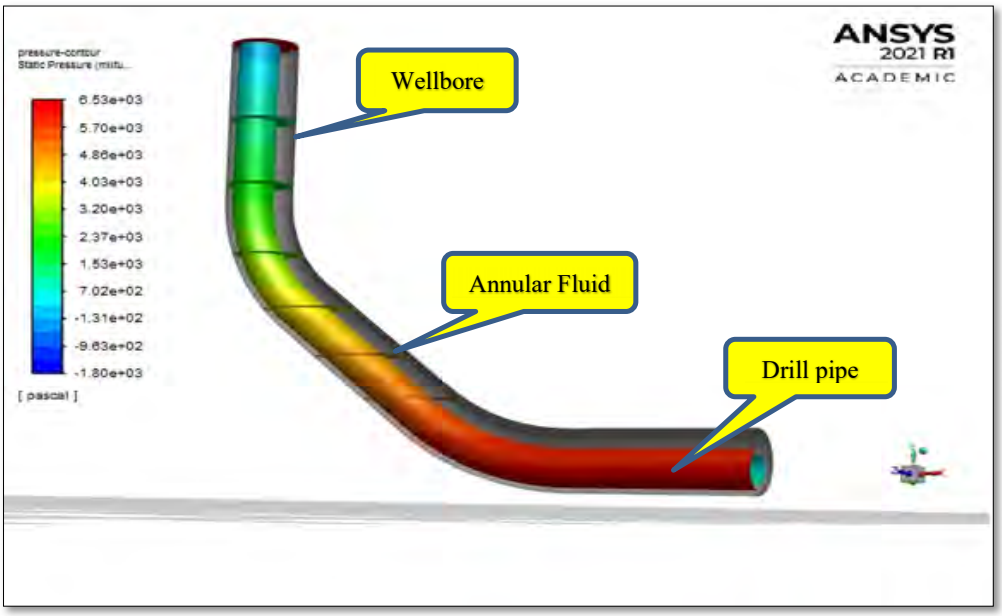

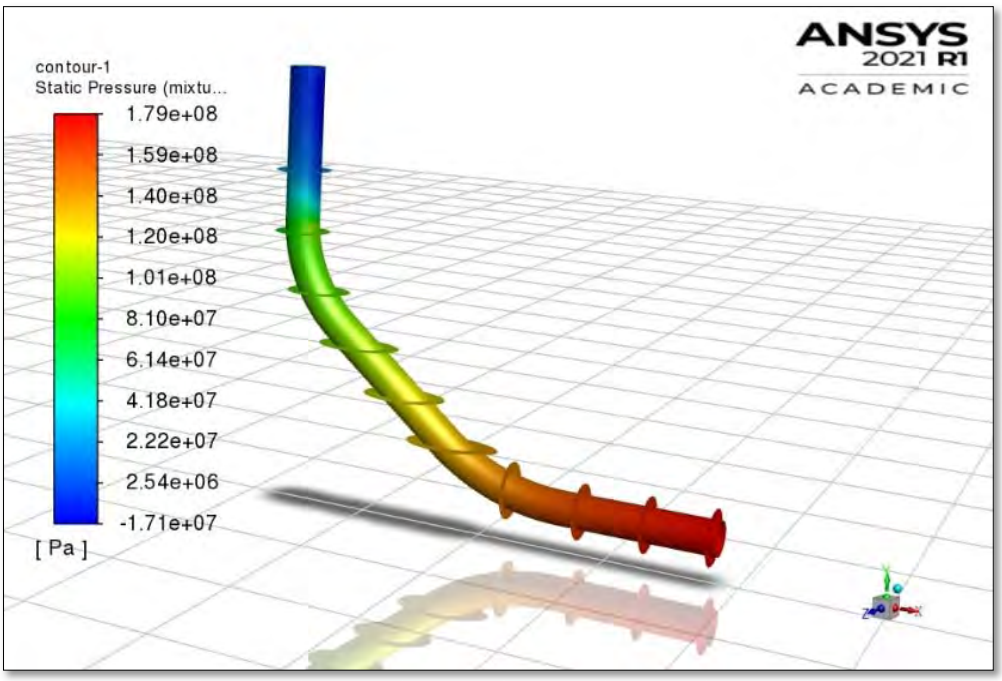

Figure 5.9: Pressure Contor

From Pressure Contor,

- Based on pressure value, it shows the high pressure zones with changes of rpm from 0 to 200 for different eccentricity.

5.6.2 Velocity Contor:

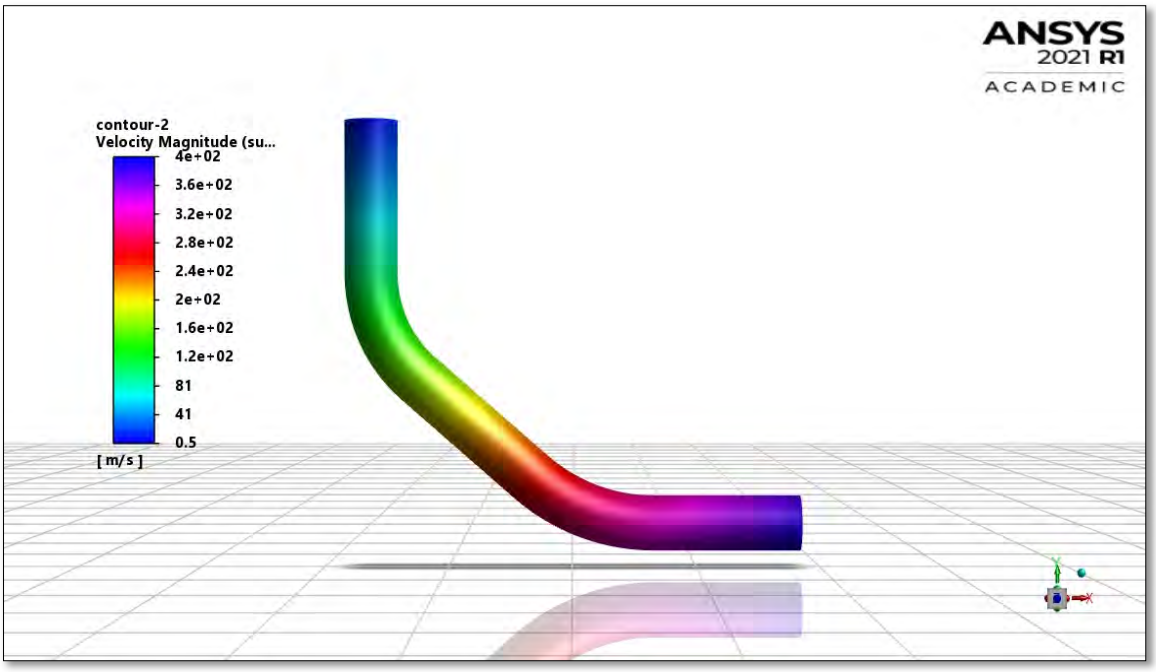

Figure 5.10: Cuttings Velocity Contor

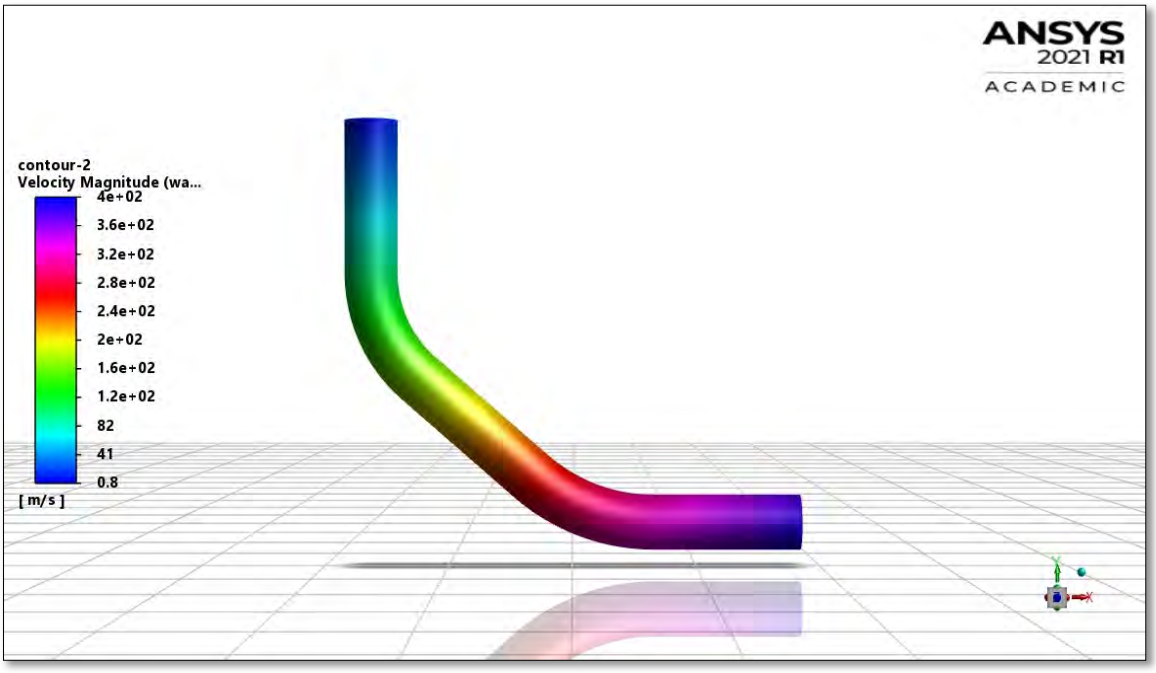

Figure 5.11: Liquid Velocity Contor

From Velocity Contour, Cutting's velocity is 0.5 m/s & Liquid velocity is 0.8 m/s.
Its been seen that the velocity at inlet is maximum & it gradually decreases with the flow. The contours graph shows different velocity regions throughout the pipe.

5.6.3 Volume fraction:

Volume fraction of a particular phase is defined as the fraction of fluid domain that is occupied by that phase. The volume of cuttings represents the amount of cutting accumulation within the fluid domain that is illustrated below for two bend at zero hole eccentricity.

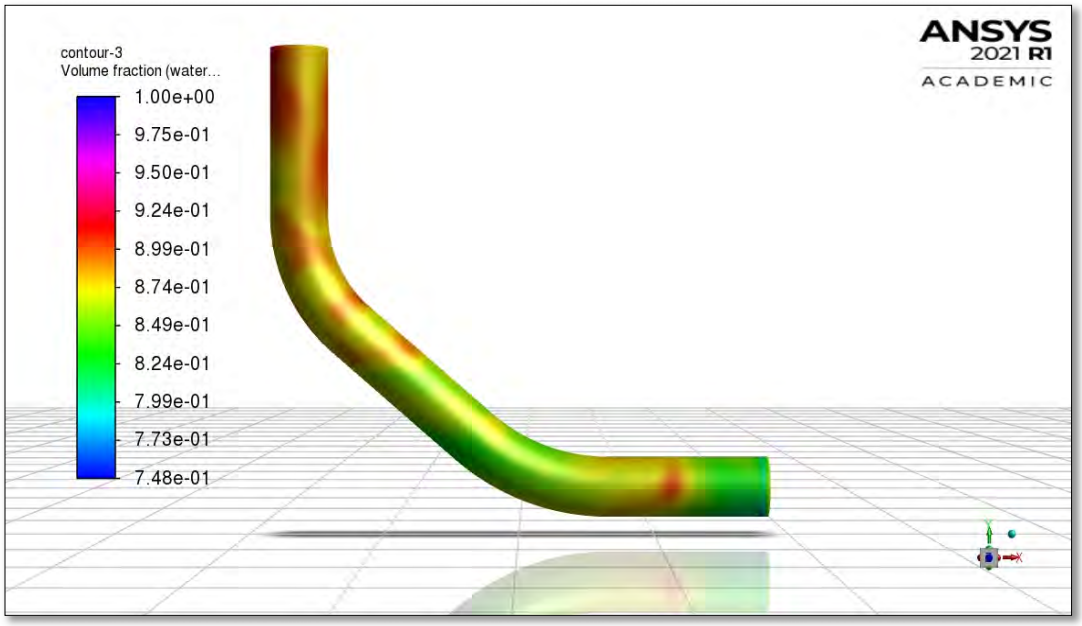

Figure 5.12: Liquid VOF at zero-hole eccentricity and 200 RPM throughout the pipe.

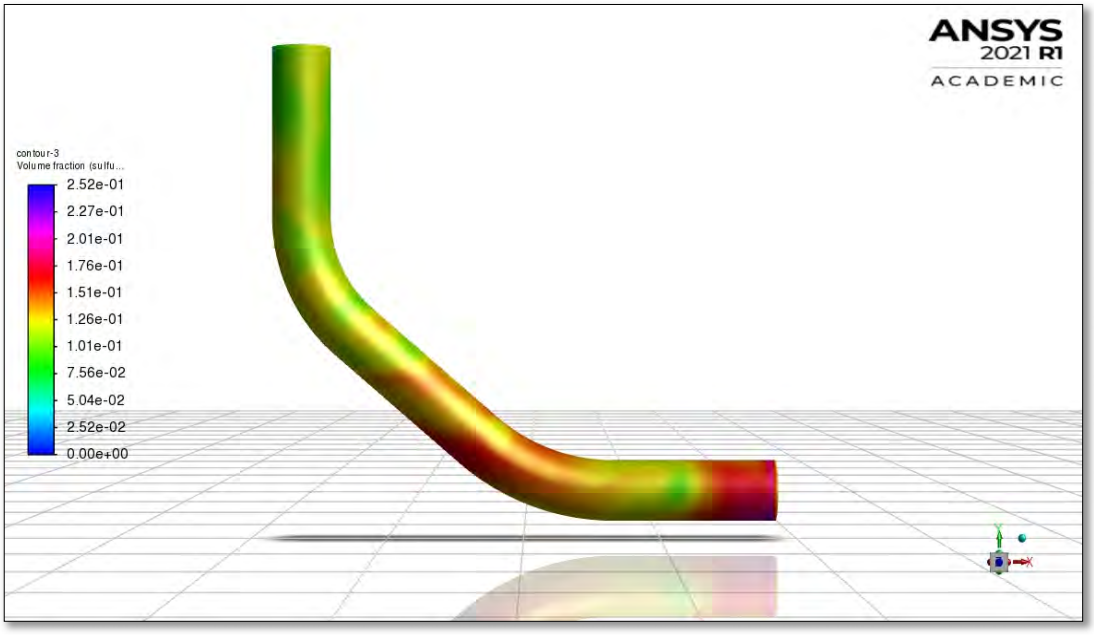

Figure 5.13: Cuttings VOF at zero-hole eccentricity and 200 RPM throughout the pipe.

From above figure,

It shows at inlet cuttings VOF is high 0.176 and it gradually decreases with the flow. At outlet VOF become 0.111 which shows the effect of RPM changes the VOF from inlet to outlet.

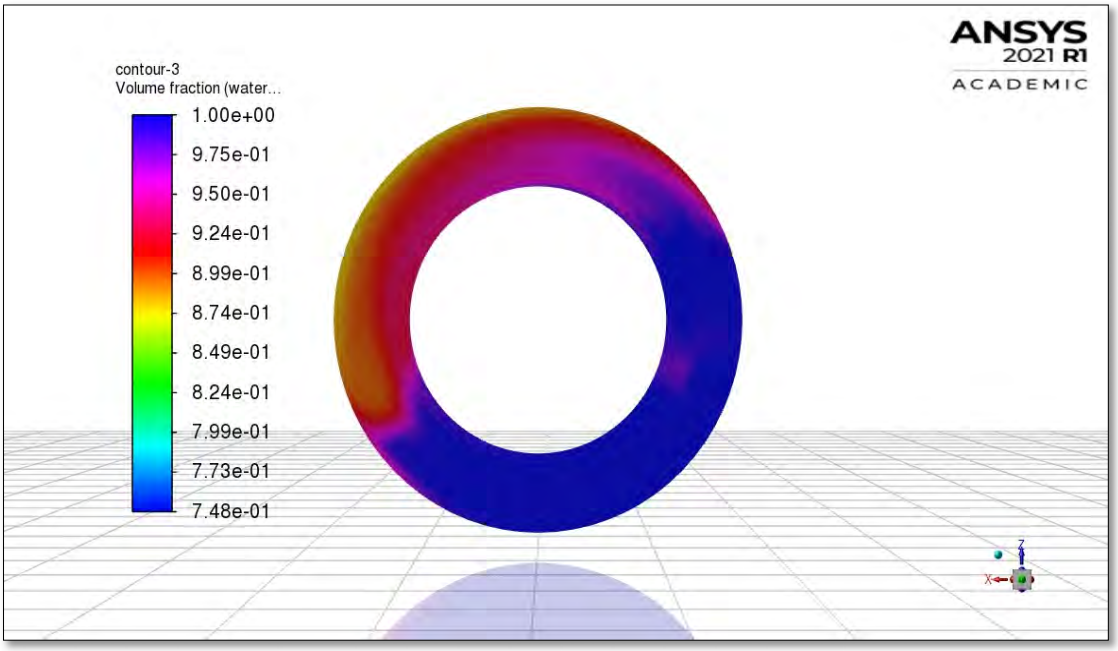

Figure 5.14: Liquid VOF at outlet at zero-hole eccentricity and 200 RPM

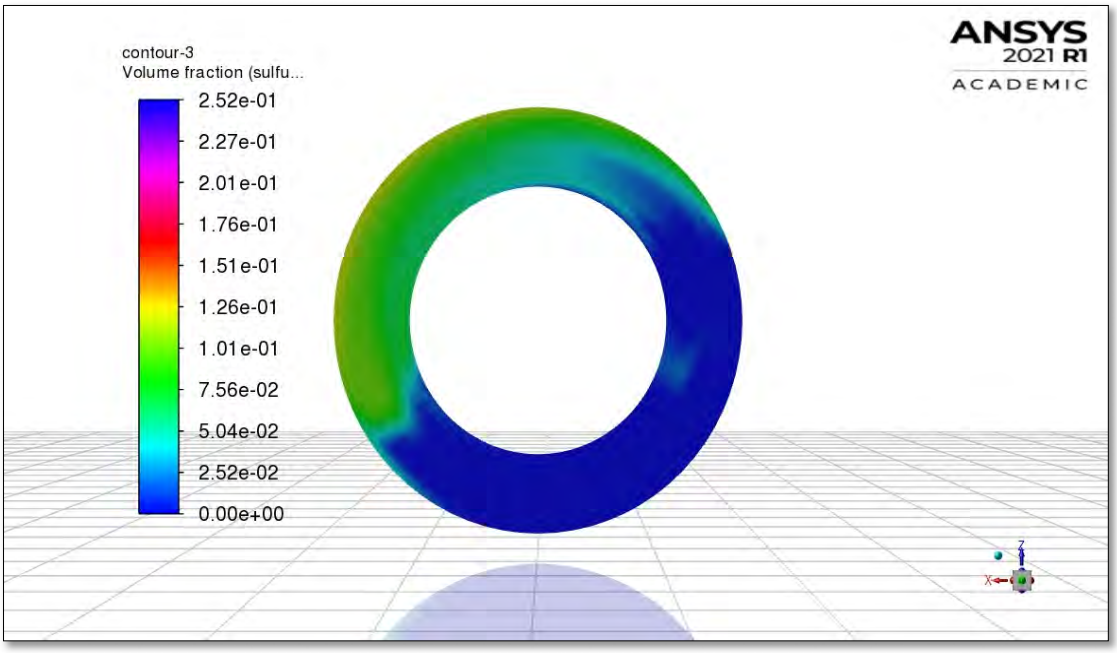

Figure 5.15: Cuttings VOF at outlet at zero-hole eccentricity and 200 RPM

From above figure,

Its been seen that the volume fraction at inlet is maximum and it gradually decreases with the flow. From the simulation the VOF at outlet becomes 0.111 whereas the VOF was 0.176 at inlet. The contours graph shows for better visualization of the effect of RPM.

5.6.4 At bend-1 (plane-4) VOF at 200 rpm with different eccentricity for both liquid & cuttings illustrate below:

At, Eccentricity, ε = 0

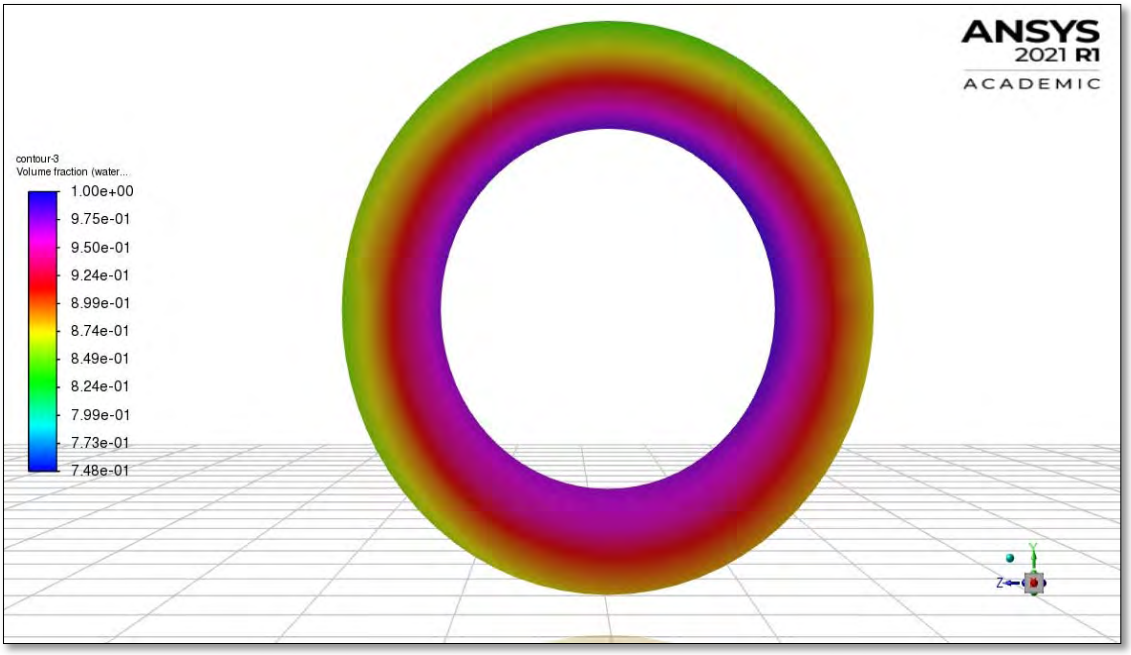

Figure 5.16: Liquid VOF at bend-1 (Plane – 4) and 200 RPM

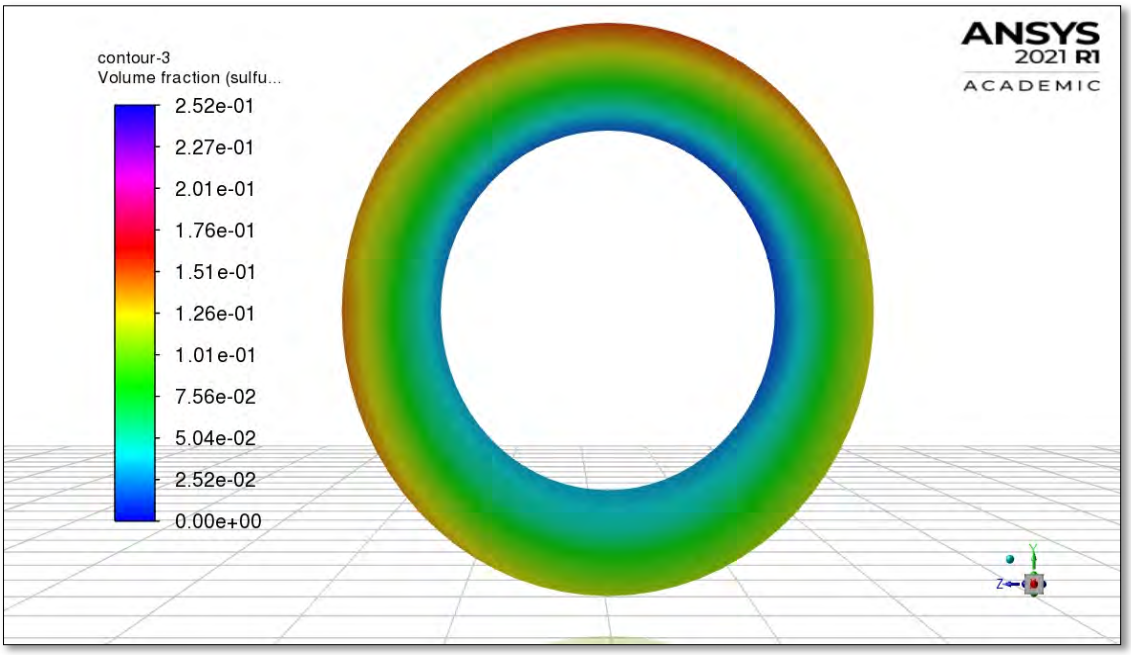

Figure 5.17: Cuttings VOF at bend-1 (Plane – 4) and 200 RPM

Initially, at bend-1 for zero-hole eccentricity and 200 RPM the cuttings VOF become 0.101 because cuttings get much space to move through the bend-1.

At, Eccentricity, ε = 0.2

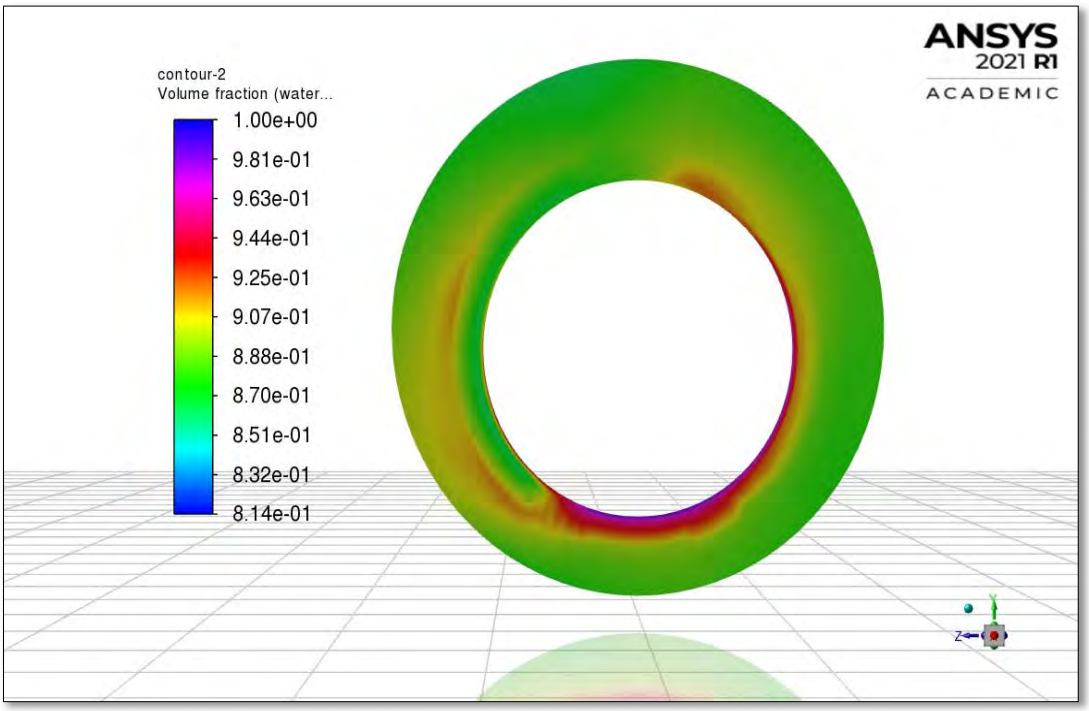

Figure 5.18: Liquid VOF at bend-1 (Plane – 4) and 200 RPM

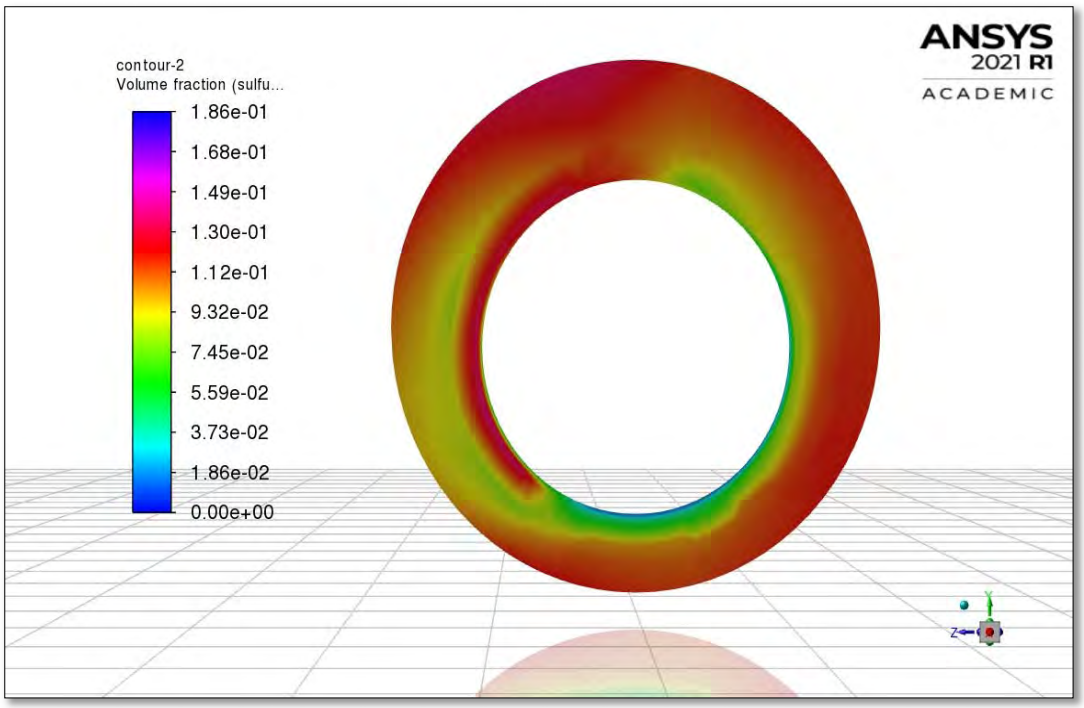

Figure 5.19: Cuttings VOF at bend-1 (Plane – 4) and 200 RPM

Initially, at bend-1 for 0.2 eccentricity and 200 RPM the cuttings VOF become 0.095 because cuttings get less space than zero-hole eccentricity to move through the bend-1.

At, Eccentricity, ε = 0.4

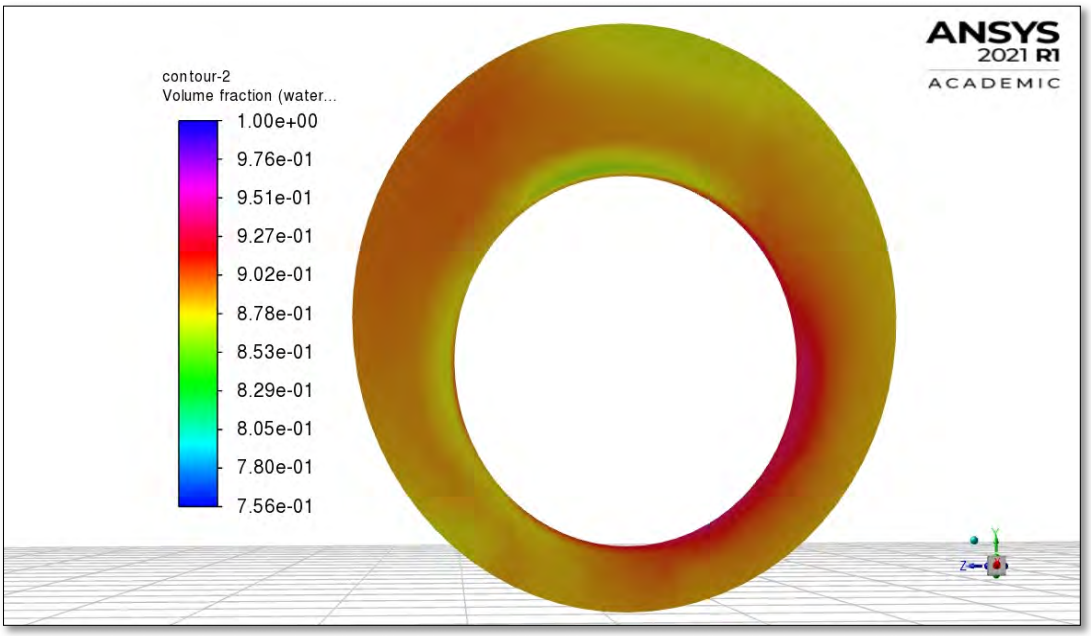

Figure 5.20: Liquid VOF at bend-1 (Plane – 4) and 200 RPM

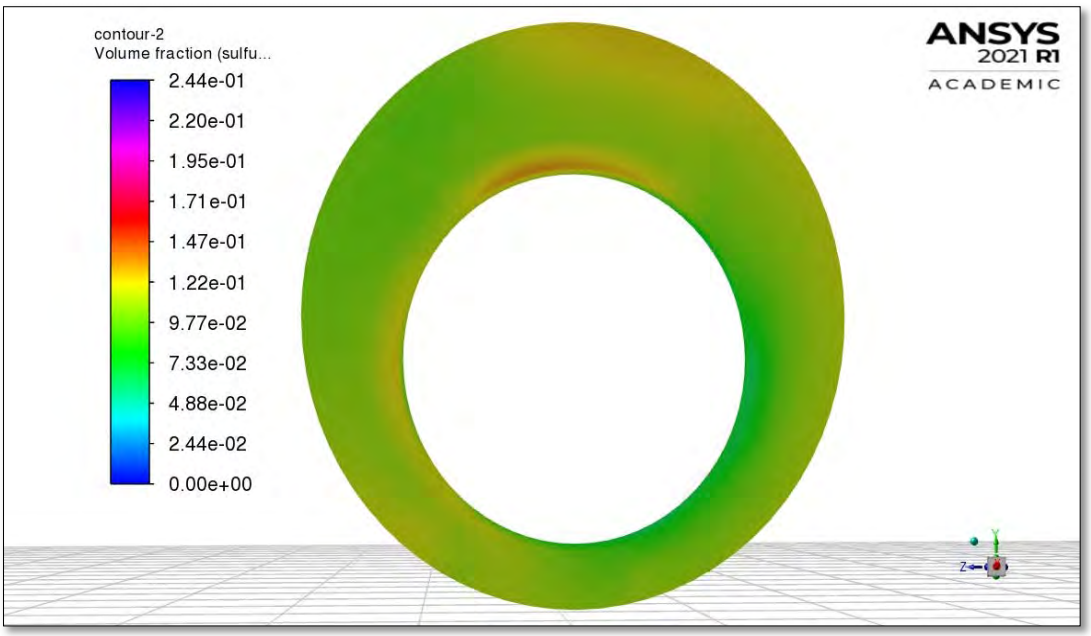

Figure 5.21: Cuttings VOF at bend-1 (Plane – 4) and 200 RPM

Initially, at bend-1 for 0.4 eccentricity and 200 RPM the cuttings VOF become 0.089 because cuttings get less space than 0.2 eccentricity to move through the bend-1.

At, Eccentricity, ε = 0.6

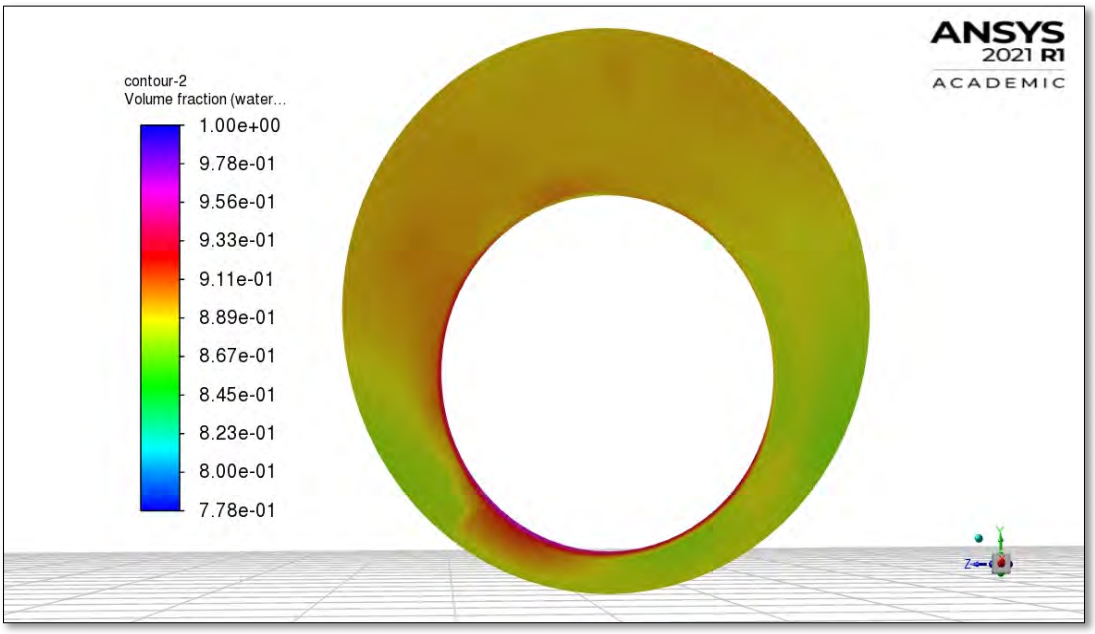

Figure 5.22: Liquid VOF at bend-1 (Plane – 4) and 200 RPM

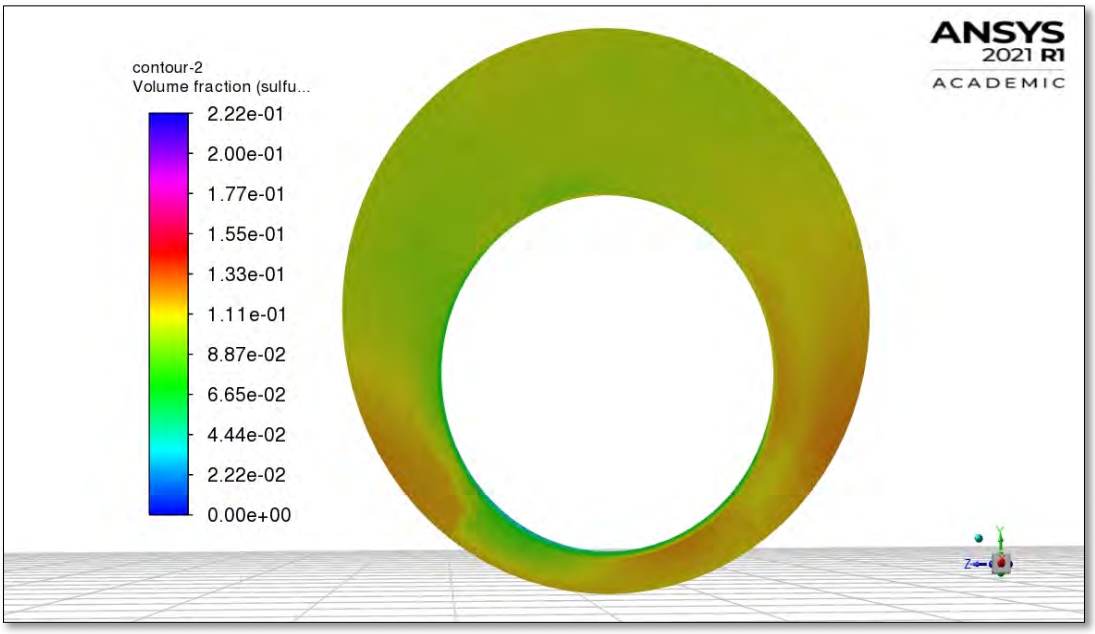

Figure 5.23: Cuttings VOF at bend-1 (Plane – 4) and 200 RPM

At bend-1 for 0.6 eccentricity and 200 RPM the cuttings VOF become 0.0887 because cuttings get less space than 0.4 eccentricity to move through the bend-1.

Its been seen that the volume fraction gradually decreases with the change of eccentricity at the same plane. At different eccentricity and 200 RPM, the simulation shows maximum VOF at zero eccentricity and then decreasing slowly at bend-1. The contours graph shows for better visualization.

5.7 Best suitable model from the simulations:

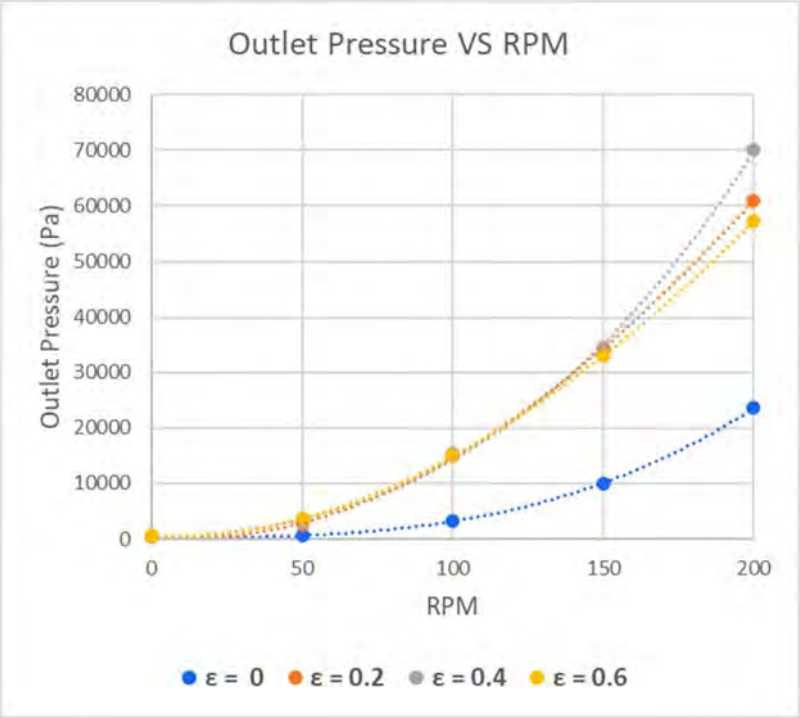

Figure 5.24: Outlet Pressure Vs RPM based on simulated results

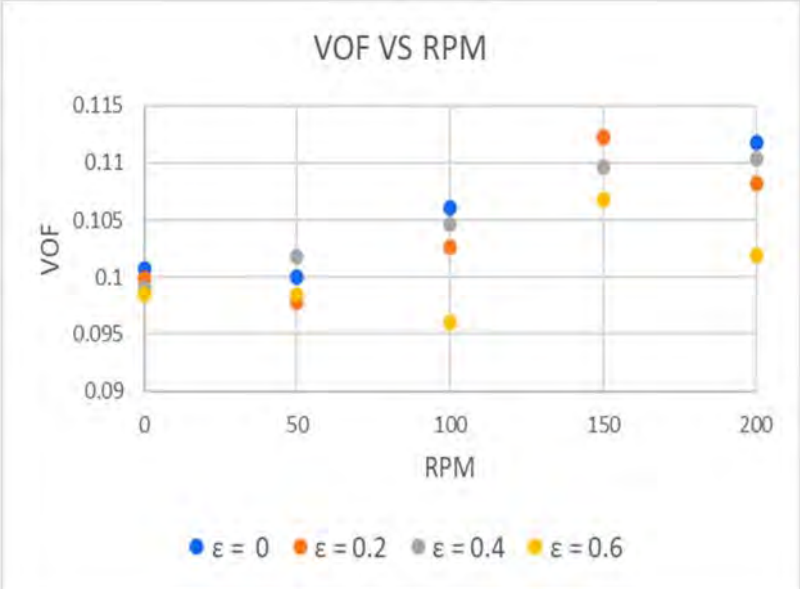

Figure 5.25: VOF Vs RPM based on simulated results

From the above models,

At eccentricity, ε = 0.4;

For 200 rpm we are getting maximum pressure 69995.22 Pa with cuttings VOF 0.1103 and with 39.64% pressure drop at bends, Which shows maximum pressure & VOF at the outlet surface. The values are shown in **Appendix.**

5.8 Model Validation:

Table-5.5: From Epelle 2018 paper (Figure-2) last graph, describes pressure drop Vs total faces for the below boundary conditions:

Cuttings Density, ρs (kg.m-3)	2800
Cuttings Diameter (m)	0.008
Fluid Inlet Velocity, Vl (m/s)	0.8
Cutting Inlet Velocity, Vs (m.s-1)	0.5
Drill Pipe Rotation, rpm	100
Hole Eccentricity, e	0.6
Initial Cutting Volume Fraction	0.1

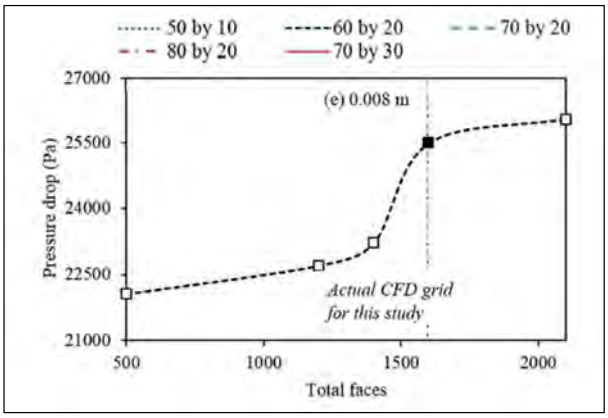

Figure 5.26: Epelle 2018 paper (Figure-2)

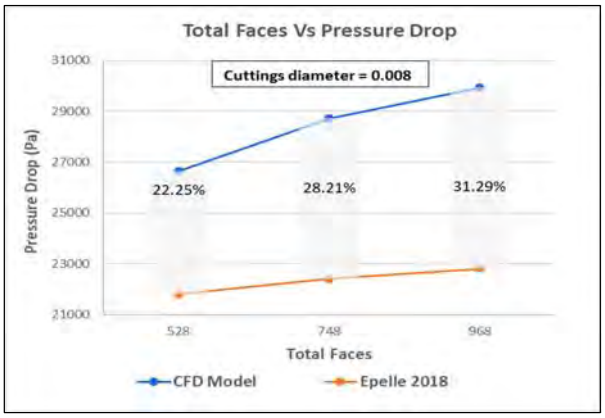

Figure 5.27: Pressure drop at outlet (For different mesh numbers).

In Figure 5.21, Epelle 2018 shows the pressure drop for different number of mesh elements, which shows a trend of increasing pressure drop with respect to mesh number.

In Figure 5.22, plot the pressure drop for different number of mesh elements considered in the simulated model which also shows a trend of increasing pressure drop with respect to mesh number. Variation in Pressure Drop from Epelle 2018;

For 528 number of faces shows 22.25% more pressure drop in the simulated model.

For 748 number of faces shows 28.21% more pressure drop in the simulated model.

For 968 number of faces shows 31.29% more pressure drop in the simulated model.

Variation in Pressure Drop due to the Number of Mesh Elements considered in the projected CFD model. In Epelle 2018, they have considered 6,65,600 number of mesh elements where in the simulated model considered 2,57,386 number of mesh elements, due to PC configuration.

5.9 REGRESSION ANALYSIS

At, Eccentricity, ε = 0.4

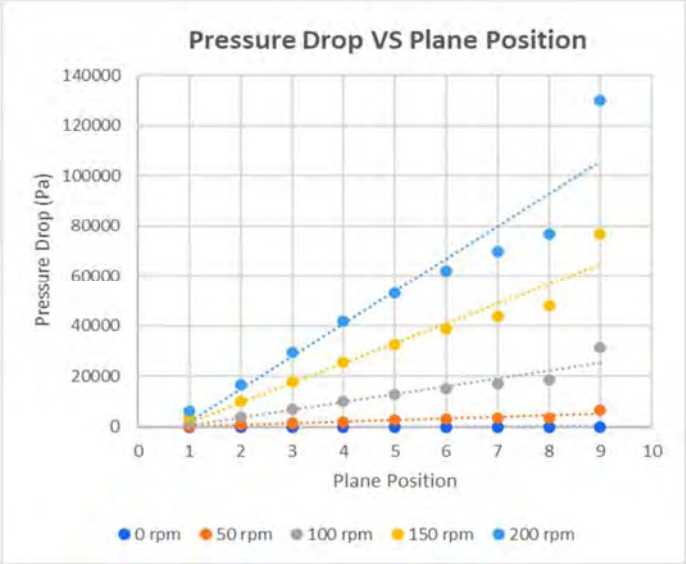

Figure 5.28: Pressure Drop at all Plane Position for 0.4 Eccentricity

Table 5.6: Regression Equation for Annular Pressure Drop (Effect of Rotation: Case-1 to 5)

RPM	Regression Equation	
0	y = 2.69x – 8.192,	R^2 = 0.4853
50	y = 606.03x – 507.45,	R^2 = 0.9037
100	y = 3000x – 3000,	R^2 = 0.9193
150	y = 8000x – 6000,	R^2 = 0.9439
200	y = 10000x – 10000,	R^2 = 0.9604

From the table,

The value of interception (c) of the regression equations (y= mx + c) is increasing with the increase of rotation that shows the pressure drop increases with the increasing rotational speed of drill pipe. The rate of increase in pressure drop along the planes is also increases with the increase of rotation as the value of slope (m) of the regression equations is also increasing with the higher rotations.

In statistics, R^2 value defines how well an equation can predict a given data set. The closer the value is to 1, the better the accuracy. It can be seen from the equations that the R^2 value for all the four curves except for 0 RPM in Figure 5.21 is almost 1. Therefore, it is reasonable to conclude that the equations are good enough to predict the values of pressure at different RPM in different planes.

Chapter 6
RESULTS AND DISCUSSION

CFD Analysis of Pressure Drop (Effect of RPM and Eccentricity Change)

For eccentric condition, as the eccentricity is increased the annular passage for the fluid domain to flow through is decreased which allows to increase the pressure drop for the planes. Because of the increased eccentricity and decreased annular gap the fluid at the entrance generates excessive pressure than the initial pressure which results in negative pressure drop in those planes.

All of these observations are valid for a lower inlet velocity that is obtained in this chapter that is for liquid 0.8 m/s and for cuttings 0.5 m/s. Observations from the relevant research regarding the pressure drop estimation along the annular trajectory also consistent with the adopted results. For a lower fluid inlet flow rate as the drill pipe rotation increases the pressure drop along the annulus also increases.

Change of bend angles for the directional drilling has a greater effect for pressure drop along the annular gap. As the bend angle of the upper bend (Bend-2) is increased 10 degrees percentage of average pressure drop has increased

For e =0 pressure drop is 50.87% at 150 RPM and 200 RPM respectively.

For e =0.2 pressure drop is 53.64% at 150 RPM and 200 RPM respectively.

For e =0.4 pressure drop is 39.64% at 150 RPM and 200 RPM respectively.

For e =0.6 pressure drop is 44.41% at 150 RPM and 200 RPM respectively.

6.1 Conclusion:

The study of multiphase flow behavior and effect of various influencing parameters in drilling operation is difficult with an experimental setup. In this study, the multiphase flow behavior of drill cuttings and effect of critical drilling parameters (bend angle, rotational speed of drill pipe, hole eccentricity) are observed applying CFD modeling to get the deep insight. Assumptions were made according to the ease of speedy computation and prepare a practical environment as much as possible considering the limitations enforced by the software.

The effect of eccentricity and pipe rotation is observed modeling a multiphase flow that involves cuttings carried out. The inlet flow velocity of liquid & cuttings are taken to be 0.8 m/s and 0.5 m/s for multiphase flow. During the multiphase flow, the solution is considered to be implicit that is independent of time.

The results obtained from simulating the flow models are consistent with conventional practices involved in drilling operations. Some input parameters are considered only for the parametric study that deviates from the practical scenario.

6.2 Summary of the findings:

The increasing rotational speed of drill pipe aids the hole cleaning as it reduces the overall cutting concentration and even at bends. The impact of modification in rotational speed is observed to be more dominant in eccentric condition of pipe compared to the concentric condition. The annular pressure drop increases with pipe rotation. Cutting particles concentrate more at bend-1 compared to bend-2 causing the increasing pressure drop at bend-1 in annuli. The hole eccentricity affects the cuttings transport efficiency adversely. Cuttings accumulate more in eccentric condition of drill pipe compared to the concentric pipes.

To diminish the adverse effect of eccentricity, the rotational speed to be much higher aiding the hole cleaning process. Turbulent flow is the best way to carrying the cuttings. Increasing the flow rate and pipe rotation enhance the cuttings transportation. Pipe rotation and fluid rheological properties have significant effect on transportation of the cuttings.

Chapter 7
RELEVANCE AND FURTHER WORK

7.1 Relevance

In the operation of drilling deviated and extended-reach wells, hole cleaning is a matter of great concern compared to the vertical wells due to the hole eccentricity and bend angle. It causes severe challenges like stuck pipe, wellbore instability, and loss in mud circulation that significantly affects the operational cost. In practical scenario, it gets more difficult to optimize the critical parameters involved in drilling when the challenges are met. Rather it is preferable to set the critical drilling parameters at optimum condition before the challenges are met considering the worst scenarios. This study involves the effect of such critical drilling parameters to provide a better understanding of optimization in aid of reducing the operational cost when the challenges are met.

7.2 Future Recommendations:

The full understanding of multi-phase flows depends strongly on the development of more efficient simulation approaches and more comprehensive experimental techniques. Some suggestions for future studies are given here to improve this study further.

More analysis with better accuracy is needed, which can minimize small errors and increase acceptance of this model for real operation. Taking the bend angles, the best possible design for the pipeline can be found. Research can be done in simultaneously with prototype set up & simulation for exact validation. Slug flow can also be analyzed in a similar manner to understand its purpose. Optimum convergent criteria analysis can be done for better results. Water and sand can be considered as non-Newtonian fluids. Formation of slug in the flow for different conditions can be analyzed. A gaseous substance can be introduced into the pipeline along with the other phases to study a three-phase flow investigation. Using better meshing can provide better results. Transient simulation can be done to get better idea about the slug formation.

REFERENCE

[1] Yasin Demiralp, Effects Of Drill-pipe Whirling Motion On Cuttings Transport Performance For Horizontal Drilling, LSU Digital Commons. (2014). https://digitalcommons.lsu.edu/gradschool_theses/2238/ (accessed February 4, 2022).

[2] [Non-Newtonian Models | Materials | SimScale, SimScale. (2021). https://www.simscale.com/docs/simulation-setup/materials/non-newtonian-models/ (accessed February 4, 2022).

[3] Abimbola, Majeed Olasunkanmi , Chukwu, Godwin , Khan, Faisal . "Cuttings Transport Evaluation in Deviated Wells." Cuttings Transport Evaluation in Deviated Wells, Proceedings of the International Conference on Marine and Freshwater Environments (iMFE2014),pp.1-10, https://journals.library.mun.ca/ojs/index.php/IMFE/article/view/1237. (2014).

[4] Joshi, Sanjay , Bhaisare, Arman , , NA . "Graphical Method to Determine Minimum CuttingFluid Velocity for Effective Hole Cleaning." Graphical Method to Determine Minimum CuttingFluid Velocity for Effective Hole Cleaning, International Research Journal of Engineering and Technology(IRJET),Vol4,pp.6, https://1library.net/document/y6j21vgq-graphical-method-determine-minimum-cutting-velocity-effective-cleani ng.html. (2017).

[5] Joshi, Sanjay , Bhaisare, Arman , , NA . "Cuttings transport in inclined and horizontal wellbore." Cuttings transport in inclined and horizontal wellbore, University of Stavanger, Norway, pp. 137, https://uis.brage.unit.no/uis-xmlui/handle/11250/183275. (2010).

[6] Tomren, P. H. , Iyoho, A. W. , Azar, J. J. . "Experimental Study of Cuttings Transport in Directional Wells ." Experimental Study of Cuttings Transport in Directional Wells , Society of Petroleum Engineers, pp. 14, https://www.onepetro.org/journal-paper/SPE-12123-PA. (1986).

[7] Yan, Tie , Shao , Shuai , Jiao , Jianjun , Sun, Xiaofeng . "Effect of drillpipe rotation on cuttings transport using computational fluid dynamics (CFD) in complex structure wells." Effect of drillpipe rotation on cuttings transport using computational fluid

dynamics (CFD) in complex structure wells, Journal of Petroleum Exploration and ProductionTechnology,Vol4,pp.255–261, https://link.springer.com/article/10.1007/s13202-014-0118-x. (2014).

[8] S. Joshi, A. Bhaisare, A. Professor, Graphical Method to Determine Minimum Cutting Fluid Velocity for Effective Hole Cleaning, n.d. https://www.irjet.net/archives/V4/i6/IRJET-V4I6552.pdf.

[9] R. Ranjbar, Cuttings transport in inclined and horizontal wellbore, Unit.No. (2017). doi:http://hdl.handle.net/11250/183275.

[10] P.H. Tomren, A.W. Iyoho, J.J. Azar, Experimental Study of Cuttings Transport in Directional Wells, SPE Drilling Engineering. 1 (1986) 43–56. doi:10.2118/12123-pa.

[11] J. Akrong, N. Abuja, EFFECT OF PIPE ECCENTRICITY ON HOLE CLEANING AND WELLBORE HYDRAULICS, 2010. https://pdfs.semanticscholar.org/2b10/fa611430a0e598b4c3961d1ef4498fc21b9e.pdf.

[12] T.N. Ofei, Modelling of Pressure Drop and Cuttings Concentration in Eccentric Narrow Horizontal Wellbore with Rotating Dr, Scialert.Net. (2014). https://scialert.net/fulltext/amp.php?doi=jas.2014.3263.3269##f7 (accessed August 26, 2020).

[13] R.A. Sultan, M.A. Rahman, S. Rushd, S. Zendehboudi, V.C. Kelessidis, CFD Analysis of Pressure Losses and Deposition Velocities in Horizontal Annuli, International Journal of Chemical Engineering. 2019 (2019) 1–17. doi:10.1155/2019/7068989.

[14] X. Sun, K. Wang, T. Yan, S. Shao, J. Jiao, Effect of drillpipe rotation on cuttings transport using computational fluid dynamics (CFD) in complex structure wells, Journal of Petroleum Exploration and Production Technology. 4 (2014) 255–261. doi:10.1007/s13202-014-0118-x.

[15] Kadri, U., Zoeteweij, M. L., Mudde, R. F., &Oliemans, R. V. A. (2009). A growth model for dynamic slugs in gas–liquid horizontal pipes. International Journal of Multiphase Flow, 35(5), 439-449.

[16] Czapp, M., Utschick, M., Rutzmoser, J., &Sattelmayer, T. (2012, July). Investigations on slug flow in a horizontal pipe using stereoscopic particle imagevelocimetry and CFD simulation with volume of fluid method. In Proc. of the 20th Int. Conf. on Nucl. Eng (Vol. 3, pp. 477-486

[17] Holland, F., & Bragg, R. (1995). Fluid Flow for Chemical and Process Engineers. Butterworth-Heinemann.

[18] Gould, T. L., Tek, M. R., & Katz, D. L. (1974). Two-phase flow through vertical, inclined, or curved pipe. Journal of Petroleum Technology, 26(08), 915-926.

[19] Brandstaetter, W., Ragab, A., &Shalaby, S. (2007). Modeling of Two-Phase Flow, and Slug Flow Characteristics in Horizontal/Inclined Pipelines using CFD.

[20] Wallis, G. B. (1969). One-dimensional two-phase flow.

[21] Kleinstreuer, C. (2003). Two-phase flow: theory and applications. CRC Press.

[22] Toda, M., & Konno, H. (1987). Fundamentals of Gas-Liquid-Solid Three-Phase Flow. Japanese J. Multiphase Flow,(in Japanese), 1(2), 139.

[23] Barnea, D., Shoham, O., Taitel, Y., &Dukler, A. E. (1985). Gas-liquid flow in inclined tubes: flow pattern transitions for upward flow. Chemical Engineering Science, 40(1), 131-136.

[24] Singh, G., & Griffith, P. (1970). Determination of the pressure drop optimum pipe size for a two-phase slug flow in an inclined pipe. Journal of Engineering for Industry, 92(4), 717-726.

[25] Ragab, A., Brandstaetter, W., &Shalaby, S. Multiphase Flows in Horizontal and Inclined Pipelines by CFD Simulations.

[26] Al-Lababidi, S., Addali, A., Yeung, H., Mba, D., & Khan, F. (2009). Gas void fraction measurement in two-phase gas/liquid slug flow using acoustic emission technology. Journal of Vibration and Acoustics, 131(6), 064501.

[27] Hossain, Dr Md Alamgir. (2012). Particle Dispersion and Deposition in Multiphase Turbulence Flow: Analytical and CFD Modeling.

[28] Buwa, V. V., Deo, D. S., &Ranade, V. V. (2006). Eulerian–Lagrangian simulations of unsteady gas–liquid flows in bubble columns. International journal of multiphase flow, 32(7), 864-885.

[29] FLUENT, A. (2010). 12.1 Theory guide, Solver Theory. ANSYS Inc.

[30] Delnoij, E., Kuipers, J. A. M., &Swaaij, W. P. M. (1998). Numerical simulation of bubble coalescence using a Volume of Fluid (VOF) model.

[31] Özbelge, T. A., &Beyaz, A. (2001). Dilute solid–liquid upward flows through a vertical annulus in a closed loop system. International journal of multiphase flow, 27(4), 737-752.

[32] Launder, B. E., Reece, G. J., &Rodi, W. (1975). Progress in the development of a Reynolds-stress turbulence closure. Journal of fluid mechanics, 68(3), 537-566.

[33] Gibson, M. M., & Launder, B. E. (1978). Ground effects on pressure fluctuations in the atmospheric boundary layer. Journal of Fluid Mechanics, 86(3), 491-511.

[34] Chorin, A. J. (1968). Numerical solution of the Navier-Stokes equations. Mathematics of computation, 22(104), 745-762.

[35] Daly, B. J., & Harlow, F. H. (1970). Transport equations in turbulence. The Physics of Fluids, 13(11), 2634-2649.

[36] Launder, B. E. (1989). Second-moment closure and its use in modelling turbulent industrial flows. International Journal for Numerical Methods in Fluids, 9(8), 963-985.

[37] Lien, F. S., &Leschziner, M. A. (1994). Assessment of turbulence-transport models including non-linear RNG eddy-viscosity formulation and second-moment closure for flow over a backward-facing step. Computers & Fluids, 23(8), 983-1004.

[38] Fu, S., Launder, B. E., Leschziner, M. A. (1987). Modelling strongly swirling recirculating jet flow with Reynolds-stress transport closures. In 6th Symposium on Turbulent Shear Flows (pp. 17-6).

[39] Karman, T. V. (1937). The fundamentals of the statistical theory of turbulence. Journal of the Aeronautical Sciences, 4(4), 131-138.

[40] Nizar, Fahim (2019) in Military Institute of Science and Technology. B.Sc thesis titled, CFD modelling of drill cuttings transport efficiency in annular bends.

[41] Sarkar, S., &Lakshmanan, B. (1991). Application of a Reynolds stress turbulence model to the compressible shear layer. AIAA journal, 29(5), 743-749.

[42] Skudarnov, P. V., Lin, C. X., Ebadian, M. A. (2004). Double-species slurry flow in a horizontal pipeline. Journal of fluids engineering, 126(1), 125-132.

[43] Wood, D. J., (1966). Civil Eng.-A.S.C.E. 36 (12), 60. Cited in Govier, G. W., Aziz. , K. (1977). The flow of complex mixtures in pipes. Krieger Pub Co.

APPNEDIX

Data for Chapter 5

Plane wise pressure and pressure drop for different rpm

Table-A1: Concentric Condition: For Eccentricity, ε = 0

Plane	0 rpm		50 rpm		100 rpm	
	Pressure (Pa)	Pressure Drop	Pressure (Pa)	Pressure Drop	Pressure (Pa)	Pressure Drop
plane-1	599.67	0.00	8014.13	0.00	38585.77	0.00
plane-2	508.48	91.19	7627.83	386.30	37010.80	1574.98
plane-3	490.02	109.66	7046.39	967.74	34451.80	4133.97
plane-4	399.06	200.62	6368.64	1645.49	31137.77	7448.00
plane-5	396.38	203.29	5589.26	2424.87	27949.84	10635.93
plane-6	393.50	206.17	4981.84	3032.29	25179.88	13405.89
plane-7	390.31	209.36	4432.00	3582.13	22323.25	16262.53
plane-8	386.00	213.68	3981.54	4032.59	19980.49	18605.28
plane-9	379.33	220.34	3538.67	4475.47	17602.78	20983.00
plane-10	347.71	251.97	622.13	7392.00	3214.19	35371.59

Plane	150 rpm		200 rpm	
	Pressure (Pa)	Pressure Drop	Pressure (Pa)	Pressure Drop
plane-1	80759.07	0.00	177732.06	0.00
plane-2	77566.89	3192.17	171084.34	6647.72
plane-3	72044.81	8714.26	160470.75	17261.31
plane-4	66324.30	14434.77	147375.46	30356.60
plane-5	59333.42	21425.65	132669.54	45062.52
plane-6	54026.03	26733.03	118667.72	59064.34
plane-7	49457.61	31301.45	107205.32	70526.74
plane-8	46378.92	34380.15	97329.56	80402.50
plane-9	42447.07	38312.00	86816.95	90915.11
plane-10	10084.35	70674.72	23586.07	154145.99

Table-A2: Eccentric Condition: For Eccentricity, ε = 0.2

Plane	0 rpm		50 rpm		100 rpm	
	Pressure (Pa)	Pressure Drop (Pa)	Pressure (Pa)	Pressure Drop (Pa)	Pressure (Pa)	Pressure Drop (Pa)
plane-1	684.35	0.00	8997.77	0.00	46315.70	0.00
plane-2	601.17	83.18	8676.62	321.15	44913.82	1401.89
plane-3	624.87	59.49	8096.87	900.90	42615.47	3700.24
plane-4	625.28	59.07	7664.44	1333.33	39340.94	6974.76
plane-5	524.97	159.39	7101.88	1895.89	36406.26	9909.45
plane-6	524.20	160.16	6584.43	2413.33	33691.80	12623.91
plane-7	523.14	161.21	6132.84	2864.93	31412.50	14903.21
plane-8	521.81	162.54	5788.70	3209.07	29532.44	16783.26
plane-9	519.96	164.40	5563.34	3434.43	27983.87	18331.83
plane-10	527.68	156.67	2666.43	6331.34	14977.70	31338.00

Plane	150 rpm		200 rpm	
	Pressure (Pa)	Pressure Drop (Pa)	Pressure (Pa)	Pressure Drop (Pa)
plane-1	110996.51	0.00	196230.77	0.00
plane-2	107390.44	3606.07	190029.09	6201.68
plane-3	101039.14	9957.37	179763.06	16467.71
plane-4	93195.85	17800.66	166992.40	29238.37
plane-5	85455.20	25541.31	154253.09	41977.68
plane-6	78359.16	32637.35	143272.50	52958.27
plane-7	72381.01	38615.50	134118.32	62112.45
plane-8	67149.32	43847.19	126485.66	69745.11
plane-9	63145.62	47850.89	119556.37	76674.40
plane-10	34224.95	76771.56	61042.00	135188.77

Table-A3: Eccentric Condition: For Eccentricity, ε = 0.4

Plane	0 rpm		50 rpm		100 rpm	
	Pressure (Pa)	Pressure Drop (Pa)	Pressure (Pa)	Pressure Drop (Pa)	Pressure (Pa)	Pressure Drop (Pa)
plane-1	699.00	0.00	10292.04	0.00	44939.70	0.00
plane-2	600.32	98.68	10247.44	44.60	44696.10	243.60
plane-3	518.97	180.02	10211.14	80.90	44502.92	436.78
plane-4	519.45	179.55	9679.46	612.58	41906.23	3033.47
plane-5	539.10	159.89	8863.40	1428.64	38696.16	6243.53
plane-6	418.35	280.64	8091.77	2200.27	35759.19	9180.50
plane-7	417.19	281.80	7428.63	2863.41	33168.79	11770.91
plane-8	395.40	303.60	6908.21	3383.83	31072.04	13867.66
plane-9	360.75	338.25	6285.33	4006.71	29044.04	15895.65
plane-10	339.32	359.68	2803.04	7489.00	15354.86	29584.84

Plane	150 rpm		200 rpm	
	Pressure (Pa)	Pressure Drop (Pa)	Pressure (Pa)	Pressure Drop (Pa)
plane-1	109591.54	0.00	203024.67	0.00
plane-2	108965.30	626.24	201865.89	1158.78
plane-3	108430.91	1160.63	200858.31	2166.36
plane-4	102338.99	7252.55	189052.15	13972.52
plane-5	94670.79	14920.75	174357.06	28667.61
plane-6	86843.37	22748.17	161308.90	41715.77
plane-7	80079.04	29512.50	149848.25	53176.42
plane-8	75233.32	34358.22	139737.04	63287.63
plane-9	70209.70	39381.84	130711.05	72313.62
plane-10	34456.90	75134.64	69995.22	133029.45

Table-A4: Eccentric Condition: For Eccentricity, ε = 0.6

Plane	0 rpm		50 rpm		100 rpm	
	Pressure (Pa)	Pressure Drop (Pa)	Pressure (Pa)	Pressure Drop (Pa)	Pressure (Pa)	Pressure Drop (Pa)
plane-1	699.68	0.00	12651.06	0.00	54804.66	0.00
plane-2	619.62	80.06	12575.34	75.72	54423.08	381.58
plane-3	649.63	50.05	12524.53	126.53	54138.74	665.92
plane-4	649.48	50.20	11921.05	730.01	51266.84	3537.82
plane-5	548.15	151.53	11235.22	1415.83	47575.43	7229.23
plane-6	545.99	153.69	10533.13	2117.92	44029.04	10775.62
plane-7	543.64	156.04	9917.99	2733.07	41168.51	13636.15
plane-8	540.42	159.26	9378.07	3272.99	38581.86	16222.80
plane-9	533.76	165.92	8713.36	3937.70	35607.87	19196.79
plane-10	559.42	140.26	3686.57	8964.49	14870.04	39934.62

Plane	150 rpm		200 rpm	
	Pressure (Pa)	Pressure Drop (Pa)	Pressure (Pa)	Pressure Drop (Pa)
plane-1	123747.49	0.00	196157.28	0.00
plane-2	122694.39	1053.10	194207.81	1949.47
plane-3	121894.01	1853.48	192707.59	3449.69
plane-4	114989.48	8758.01	181752.86	14404.42
plane-5	107372.92	16374.57	171156.97	25000.31
plane-6	99905.69	23841.81	161279.57	34877.71
plane-7	93284.96	30462.54	152122.44	44034.84
plane-8	87317.07	36430.43	145400.75	50756.53
plane-9	80591.09	43156.40	138606.38	57550.90
plane-10	33014.08	90733.41	57238.88	138918.40

Table-A5: Pressure at outlet for different eccentricity and rpm

RPM	ε = 0	ε = 0.2	ε = 0.4	ε = 0.6
0	347.71	527.68	339.32	559.42
50	622.13	2666.43	2803.04	3686.57
100	3214.19	14977.70	15354.86	14870.04
150	10084.35	34224.95	34456.90	33014.08
200	23586.07	61042.00	69995.22	57238.88

Table-A6: VOF for different eccentricity and rpm

RPM	ε = 0	ε = 0.2	ε = 0.4	ε = 0.6
0	0.1007279	0.09993117	0.09910565	0.09846874
50	0.1000145	0.0978052	0.1018561	0.09852962
100	0.1060562	0.1026774	0.1046907	0.09604234
150	0.1122634	0.1121859	0.1096179	0.1067943
200	0.1117692	0.1082018	0.1103406	0.1019204

Table-A7: Total faces Vs pressure drop

Total Faces	Epelle 2018	CFD Model
528	21800	26651.8
748	22400	28719.9
968	22800	29934.6